博士論文

Rapid detection of SARS-CoV-2 RNA using Reverse Transcription Recombinase Polymerase Amplification (RT-RPA) with Lateral Flow for N-protein gene and variant-specific deletion-insertion mutation in S-protein gene

（逆転写リコンビナーゼポリメラーゼ増幅法（RT-RPA）とラテラルフロー法を用いた新型コロナウイルス RNA の N タンパク遺伝子、および変異株特異的 S タンパク遺伝子の欠失・挿入部の迅速な検出法）

東北大学大学院医学系研究科医科学専攻

病理病態学講座微生物学分野

Jose Luis Malaga Granda

Content

1. Summary

Rapid molecular testing for severe acute respiratory syndrome coronavirus 2 (SARS-CoV-2) variants may contribute to the development of public health measures, particularly in resource-limited areas. Reverse transcription recombinase polymerase amplification using a lateral flow assay (RT-RPA-LF) allows rapid RNA detection without thermal cyclers. In this study, we developed two assays to detect the SARS-CoV-2 nucleocapsid (N) gene and Omicron BA.1 spike (S) gene-specific deletion–insertion mutations (del211/ins214). Both tests had a detection limit of 10 copies/µL *in vitro* and the detection time was approximately 35 min from incubation to detection. The sensitivities of SARS-CoV-2 (N) RT-RPA-LF by viral load categories were 100% for clinical samples with high (> 9015.7 copies/µL, cycle quantification (Cq): < 25) and moderate (385.5–9015.7 copies/µL, Cq: 25–29.9) viral load, 83.3% for low (16.5–385.5 copies/µL, Cq: 30–34.9), and 14.3% for very low (< 16.5 copies/µL, Cq: 35–40). The sensitivities of the Omicron BA.1 (S) RT-RPA-LF were 94.9%, 78%, 23.8%, and 0%, respectively, and the specificity against non-BA.1 SARS-CoV-2-positive samples was 96%. The assays seemed more sensitive than rapid antigen detection in moderate viral load samples. Although implementation in resource-limited settings requires additional improvements, deletion–insertion mutations were successfully detected by the RT-RPA-LF technique.

Keywords: SARS-CoV-2, variant of concern (VOC), deletion-insertion mutation, COVID-19, recombinase polymerase amplification (RPA).

2. Introduction

2.1. SARS-CoV-2

The severe acute respiratory syndrome coronavirus 2 (SARS-CoV-2) belongs to the Nidovirales order, Coronaviridae family, Coronavirinae subfamily and Betacoronavirus genus, sharing more than 90 % of amino acid identity on the sequence of the replicase conserved domains with other coronavirus belonging to the same genus, including the SARS-CoV, MERS-CoV, and the common cold human coronaviruses hCoV-OC43, hCoV-HKU-1 [1]. The infectious particle of the SARS-CoV-2, also known as the virion, consists of an envelope composed of the structural proteins Spike (S), Envelope (E), membrane (M), and nucleocapsid (N) [2]. The genetic material of the virus is organized as a positive-sense, single-stranded ribonucleic acid (RNA) containing approximately 30,000 nucleotides (nt). The two-thirds in the region 5' end of the genome contains the open reading frames 1a and 1b, responsible for coding proteins related to virus replication, the one-third in the region 3' codifies for structural proteins and eight accessory genes [3].

During the early stages of the pandemic, several genes were proposed as targets for the molecular detection of SARS-CoV-2, including the orf1(a,b) region, envelope (E), nucleocapsid (N), spike (S), and reverse dependent RNA polymerase (RdRp) [4]. The nucleocapsid gene was proposed by the CDC in the United States [5], since it showed lower mutation rates and a relatively more conserved region [6]. Additionally, previous studies on coronaviruses demonstrated that the level of messenger RNA expression (mRNA) of the

Nucleocapsid gene is at least 3—10 times higher than other structural proteins during the first 12 hours after infection [7].

Further studies showed that the nucleocapsid gene proved to be one of the most accurate markers for the detection and frontline screening of SARS-CoV-2 [8]. However, it is now known that depending on a specific region, the nucleocapsid gene also exhibits mutation rates similar to other genes such as S or RdRp. On the other hand, being the non-structural proteins (NSP) are the most stable for genetic mutation [9].

The SARS-CoV-2 enters the host cell by interacting with the human Angiotensin Converting Enzyme 2 (hACE2) through its Spike glycoprotein [10]. The Spike glycoprotein is a major target for neutralizing antibodies, therapeutic monoclonal antibodies, and vaccine development. It is composed of homotrimers that extend from the viral surface, giving it a crown-like appearance. The full-length protein consists of 1273 amino acids and comprises two functional subunits: subunit one (S1) and subunit two (S2). S1 is responsible for binding to the host cell receptor and contains the N-terminal domain (NTD) and receptor binding domain (RBD). S2 is involved in fusing the viral membrane with the host cell membrane. It consists of the fusion peptide (FP), heptad repeat 1 (HR1), central helix (CH), connector domain (CD), heptad repeat 2 (HR2), transmembrane domain (TM), and cytoplasmic tail. To facilitate the fusion of the virus membrane and the host cell, the S1 and S2 subunits undergo a cleavage process at a specific region known as the S1/S2 furin-cleavage site (FCS), which is mediated by the transmembrane serine protease 2 (TMPRSS2) [2]. The SARS-CoV-2 recognizes hACE2 through the

RBD, which requires the Spike protein to adopt an "up" conformation, exposing the RBD on the surface of the Spike protein [10].

The evolutionary mechanism of SARS-CoV-2 has led to the emergence of various mutations. In early 2020, the first mutation to demonstrate a fitness advantage was the D614G mutation in the Spike protein [11]. This mutation has been associated with higher viral loads [11] and has shown an approximately 20% increase in infectivity compared to previous variants [12].

Since October 2020 variants with multiple mutations, particularly in the Spike protein, have been reported. These mutations have been found to affect both infectivity and transmissibility [13]. However, now we known that mutations in the Spike protein are not the sole contributors to improved viral fitness [13].

To identify variants that exhibit significantly altered pathogenicity or immune escape, the World Health Organization (WHO) established the convention of variants of concern (VOC) and emphasized the importance of monitoring these variants continuously. These variants have been designated with specific letters of Greek alphabet [14], such as Alpha (Pango lineage B.1.17), Beta (B.1.351), Gamma (P.1), Delta (B.1.351), and Omicron (B.1.1.529), along with sub-lineages like BA.1, BA.2, BA.3, BA.4, and BA.5. This classification allows for a focused approach in tracking and studying these variants.

2.2. SARS-CoV-2 Omicron variant of concern

Omicron variant (B.1.1.529) was first reported in Africa in November 2021 [15] and rapidly became a worldwide dominant VOC by early 2022 [16]. Consequently, the Omicron subvariants emerged and the global prevalence of

the subvariants is reported as half for XBB.1.5 (47.5%), followed by XBB.1.16 (8.6%), XBB.1.9.1 (12.4%), XBB.1.9.2 (3.8%), XBB.2.3 as of May 7th, 2023 [17]. The XBB.1.5 is the most reported subvariant in American and European regions, while XBB.1.16 and XBB.1.9.1 is dominating South-East Asia and Eastern Mediterranean regions, respectively. In the African and Western Pacific regions, similar proportions of different XBB subvariants are circulating. However, a reduction in testing and genomic surveillance challenges the assessment of the subvariants, which may be of particular concern in low-resource settings.

Omicron variant (B.1.1.529) had > 30 mutations on the spike gene (S) [18]. It is characterized to have three deletions (del69, del143—145, del211) and insertion 214 (ins214) in the N-terminal domain. The deletion del143—145 promotes immune evasion [19] and the ins214 in combination with Y145D shows seven-fold resistance to antibodies [20]. The mutations D614G+P681H are known to promote TMPRSS2-independent viral entry, which probably increased the COVID-19 cases with upper respiratory tract infection [20]. The Omicron subvariant XBB.1.5, a variant of interest (VOI) has a specific mutation of S486P associated with increased ACE2 affinity [21]. Recently, XBB1.16 (VOI) with additional mutations E180V, F486P, and K478R has been spreading without additional public health risk to XBB1.5 [22].

2.3. Recombinase Polymerase Amplification RPA

Isothermal nucleic acid amplification methods are a set of techniques that allow the amplification of nucleic acids at a constant temperature. Unlike PCR, which requires temperature changes for denaturation (92 °C), annealing (62 °C), and elongation (72 °C) steps, isothermal methods achieve nucleic acid amplification at one step under a stable temperature and simpler conditions, avoiding the use of thermal cycler. Different isothermal methods show distinct characteristics, differing on their principle, number of primers, and complexity of design, hence showing different advantages and disadvantages. Among those most well know isothermal methods are recombinase polymerase amplification (RPA), loop-mediated amplification (LAMP), nucleic acid-based amplification (NASBA), and exponential strand displacement amplification [23].

RPA method was developed by Piepenburg [24], it allows rapid, sensitive, and specific nucleic acid amplification at low and constant temperatures (25 to 42 °C)Click or tap here to enter text.. The RPA relies on the mechanism of genetic recombination where two DNA molecules are exchanged at homologous regions using recombinase enzymes [25]. The DNA-strand exchange Recombinase (UvsX) bind to oligonucleotide primers in presence of ATP, forming a nucleoprotein complex that search and exchange DNA strands at specific primer-complementary sequences at DNA template strand (Figure 1a).

The nucleoprotein complex replace the complementary strand at target site forming a D-loop structure, which is stabilized by single-stranded DNA binding proteins (SSB) (Figure 1b), the DNA Polymerase will anneal the primers and synthesize new DNA from the 5' to 3' direction (Figure 1c, d), as a result, a specific exponential amplification of the target is achieved at constant temperature. (Figure 1e).

Notably, various developments in RPA have been assessed for the detection of pathogens that cause infectious diseases such as *Fasciola hepatica* [26], *Plasmodium falciparum* [27], *Cryptosporidium spp* [28] parasites, *Mycobacterium tuberculosis*. [29] and viruses such Ebola virus [30], Influenza A virus, Influenza B virus [31] and Chikungunya virus[32,33].

Recently, RPA has been developed for the rapid molecular detection of Delta variant specific mutation R203M and other three VOC-specific mutations, using a multi-step procedure that showed high accuracy in clinical samples taking about 60 minutes [34,35]. Similarly, a single-copy sensitive assay for Delta mutation L452R using a two-step showed a reaction time of 75 minutes [36]. Therefore, a single-step assay with less reaction time would be useful.

In addition to RPA, the isothermal method LAMP was developed by Notomi [37], which allows simultaneous amplification of six segments across the template sequence. It was referred to as an effective tool for the diagnosis of SARS-CoV-2, including in middle- and low-income countries [38].

However, RPA presents some advantages compared to LAMP. Among them, RPA has a relatively lower limit of detection, being reported ranging from 1 to 10 copies/µL [23,39] while it is 10 to 10^9 copies/µL for LAMP [23,40] . LAMP requires a laborious and complex primer design; considering factors such as the distance between the six target genes and primer melting temperatures for at least four different primers. As a result of such complexity in primer design and optimization, LAMP showed a rate of primer design/development of 67% compared to 100 % for RPA [41].

On the other hand, RPA shows a simpler primer design and optimization process, only requiring a set of primers of two primers without the need to consider melting temperature. This reduces the number of optimization experiments hence the test developing time is also expected to be reduced.

In addition, although I could not be included in this study, the RPA can be adapted more rapidly to a multiplex system compared to LAMP, allowing for the simultaneous detection of multiple target genes [42]. Therefore, testing SARS-CoV-2 detecting N gene and testing variants by S gene or testing two variants at the same time will be possible using lateral flow methods.

The relatively higher sensitivity, shorter test developing time, and rapid test and multiplex capability are ideal advantages in a scenario where there is a need to promptly design molecular tests in response to the emergence of new SARS-CoV-2 variants.

2.4. Problem statement and relevance of this study

Developing sensitive and specific diagnostic tests is crucial for identifying infected persons to isolate and intervene in the transmission spread [43,44]. Molecular diagnosis using real-time reverse transcription polymerase chain reaction (real-time RT-PCR) has been widely used for COVID-19 diagnosis and is mainly based on the detection of the partial nucleocapsid (N) protein region. Whole viral genome sequencing has also been conducted to monitor VOC, such as Alpha, Beta, Delta, and Omicron, and to understand viral evolution patterns [45]. Despite the implementation of the COVID-19 vaccination program, the emergence of new variants and subvariants has led to several surges in cases [46].

Although next-generation sequencing (NGS) is widely used at an unprecedented level, the coverage of genomic surveillance based on sequencing remains variable among countries, especially in low- and middle-income countries, owing to limited resources [47]. Mutation-specific real-time RT-PCR assays have also been implemented for the detection of VOCs [48–50], thus reducing the time and cost of VOC monitoring, however, the need of thermal cycler and implemented laboratories may limit its application, especially in low-resource-settings. On the other hand, the SARS-CoV-2 antigen rapid detection test (Ag-RDT) possesses favorable characteristics of low-cost, point-of-care, and rapid testing. However, it has relatively low sensitivity in clinical samples

with low or moderate viral loads [51,52]. To the best of my knowledge, this method has not yet been adapted to detect specific VOCs.

2.4.1. Study Objectives

1. To develop a rapid molecular test for the detection of the SARS-CoV-2 nucleocapsid protein gene using reverse transcription recombinase polymerase amplification, SARS-CoV-2 (N) RT-RPA-LF.
2. To perform the diagnostic evaluation of the SARS-CoV-2 (N) RT-RPA-LF using respiratory clinical samples.
3. To develop a test concept for the detection of deletions-insertions present in Omicron BA.1 VOC using recombinase polymerase amplification.
4. To perform the diagnostic evaluation of the Omicron BA.1 (S) using RT-RPA-LF on human respiratory clinical samples.

3. Materials and Methods

In this study, I developed two rapid molecular tests for the detection of the SARS-CoV-2 nucleocapsid gene and a variant-specific Omicron BA.1 using deletion and insertion as molecular markers. The development process consisted of primer design (1) for the SARS-CoV-2 nucleocapsid (N) and Spike (S) genes, a primer selection (2) using positive controls based on plasmid DNA controls, determination of limit of detection (3) testing RNA standards, cross-reactivity evaluation (4) testing nucleic acid (DNA/RNA) from some of the most common human respiratory viruses, and test accuracy evaluation (5) assessing sensitivity and specificity testing clinical samples. The sensitivity was evaluated

according to different viral load categories, including high, moderate, low, and very low viral loads.

3.1. Primer design

3.1.1. Nucleocapsid Gene

For molecular diagnosis of SARS-CoV-2, a conserved region of the N gene has been used and found to be sensitive [5,53]. Therefore, I designed two RPA primers to amplify a 166 nucleotide (nt) segment of the SARS-CoV-2 N gene (GenBank: LC523807.1) (Figure 2). Primer-BLAST was performed following the TwistAmp DNA Amplification Kits Assay Design Manual [54]. A 46 nt long probe was designed to have a fluorescein isothiocyanate molecule (6-FITC) at 5', an abasic site (d-pacer) at probe nucleotide position 31, and a C3-dSpacer at 3' end. The reverse primer was modified to include a biotin molecule at 5'. The primers and probe were synthesized by FASMAC (FASMAC, Kanagawa, Japan).

3.1.2. Spike Gene

I selected the Omicron BA.1 specific deletion-insertion mutation, del211/ins214 in the S gene, for the primers and probes design (Figure 3a). Among SARS-CoV-2 sequences downloaded from the Global Initiative on Sharing All Influenza Data (GISAID) [55] from January 15 to February 17, 2022, 57 were classified as Omicron BA.1 using the Pangolin COVID-19 Lineage Assigner [56]. Multiple sequence alignment was performed against the SARS-CoV-2 reference strain (MN908947.3) using MEGA, Version 7.0 [57]. A 394-nucleotide consensus sequence of Omicron BA.1 was named

“S_211del+214ins_deleted” (Table 1) and used to design SARS-CoV-2 specific primers. In addition, probes were designed by aligning a 46 nt segment covering the del211/ins214 (Figure 3b). The probe included a fluorescein isothiocyanate molecule (6-FITC) at the 5' end, an abasic residue (d-spacer) located after the ins214, and a C3-dSpacer at the 3' end. It was expected that annealing of the probe to the del211/ins214 segment would allow the endonuclease IV to cleave the abasic residue (d-spacer) (Figure 3c), releasing the C3-dSpacer (Figure 3d), allowing the DNA polymerase to synthesize complementary DNA from 5' to 3' end (Figure 3e). A no proper alignment of the probe and the template sequence containing the del211/ins214 may produce a loop structure exposing a single-stranded DNA, which will inhibit the cleavage activity of the end IV on the abasic residue, showing a negative result for Omicron BA.1 (Figure 3f). The RPA amplicons synthetized containing the FITC and Biotin tags will be further detected using immunochromatographic lateral flow strips (Figure 3g). The reverse primer included a biotin molecule at the 5' end. Primers and probes were synthesized at FASMAC (FASMAC, Kanagawa, Japan).

3.2. Primer selection

For the selection of the RPA primers, I evaluated the presence of amplification bands testing the primers with controls containing the SARS-CoV-2 nucleocapsid and spike genes.

3.2.1. Controls for Nucleocapsid Gene

The 2019-nCoV_N_Positive Control (IDT; Catalog#10006625) (IDT, Coralville, IA, USA) was used as a positive control for the initial primer selection process.

3.2.2. Synthesis of positive control for Omicron BA.1 Spike Gene

To generate the positive control for the Omicron BA.1 (S) RT-RPA-LF assay, I selected a 394 nucleotides sequence ranging the 21952nt-22345nt of Omicron BA.1(OL822906.1) (Table 1). The sequence was ordered to be cloned in a 2966 bp plasmid vector pUCFa (FASMAC, Kanagawa, Japan). This plasmid was utilized as a DNA-positive control and named "S_211del+214ins_deleted". The positive control was resuspended with100 µL of TE buffer, and the DNA concentration was quantified using Qubit2.0 Fluorimeter (Invitrogen, Waltham, MA, USA). The copy number was calculated as referred elsewhere [58] and 10-fold dilutions were prepared to obtain a stock of 10^5 copies/µL. Aliquots were prepared and stored at -80 °C until further utilization.

3.2.3. Synthesis of negative control (wild-type) for Spike Gene

Similarly, I selected a 395-nucleotide sequence located at 21984—22378 nt from SARS-CoV-2 showing a wild-type (OL817641.1) segment for the mutation del211/214ins (Table 1). The segment was set to be cloned on a 2966 bp plasmid vector pUCFa (FASMAC, Kanagawa, Japan). The plasmid was utilized as a DNA-negative control for the Omicron BA.1 (S) RT-RPA-LF. The plasmid was resuspended on 100 µL of TE buffer. After DNA quantification, the copy

number was calculated as referred elsewhere [58] and 10-fold dilutions were prepared equivalent to 10^3 copies/µL. The aliquots were stored at -80 °C until further utilization.

3.2.4. Primer test for the Nucleocapsid Gene

To evaluate the two RPA primers designed for a partial segment in the nucleocapsid gene, a master mix was prepared for each primer sets RPA_N1 and RPA_N2. The primers were evaluated using the TwistAmp® Basic RPA kit. The reaction mixes contained the lyophilized pellet enzymes provided in the RPA kit, 29.5 µL of rehydration buffer, 2.4 µL of forward primer (480nM), 2.4 µL of reverse primer (480nM), 5 µL of template, 8.2 µL of nuclease-free water, and 2.5 µL of Magnesium Acetate (14nM) to obtain a final volume of 50 µL. The 2019-nCoV_N_Positive Control (10^5 copies/µL) was used as a positive control (PC), and nuclease-free water was used as a non-template control (NTC). The RPA mixture was incubated at 37 °C for 30 minutes using a block heater CTU-N (Taitec Co, Ltd, Tokyo, Japan). Then the mixture was homogenized using a vortex and spun down in a microcentrifuge for 3 to 5 minutes. The amplification products were resolved using 3% gel electrophoresis.

3.2.5. Primer test for the Spike Gene

To evaluate the three RPA primer sets designed in this study for a partial segment in the Spike gene, a master mix was prepared for each primer set. The primers were evaluated using the TwistAmp® Basic RPA kit. The reaction mixes contained the lyophilized pellet enzymes provided in the RPA kit, 29.5

µL of rehydration buffer, 2.4 µL of forward primer (480nM), 2.4 µL of reverse primer (480nM), 5 µL of template, 8.2 µL of nuclease-free water, and 2.5 µL of Magnesium Acetate (14nM) to obtain a final volume of 50 µL. The Omicron BA.1 DNA plasmid (10^5 copies/µL) was used as a positive control (PC), and nuclease-free water was used as a NTC. The RPA mixture was incubated at 37 °C for 30 minutes using a block heater CTU-N (Taitec Co, Ltd, Tokyo, Japan). Then the mixture was homogenized using a vortex and spun down in a microcentrifuge for 3 to 5 minutes. The amplification products were resolved using 3% gel electrophoresis.

The primer Set2 was further evaluated for the limit of detection testing 10-fold dilutions of the positive control, with concentrations equivalent to 10^5, 10^4, 10^3, 10^2, 10, and 1 copy/µL.

To evaluate if the probes worked properly, two master mixes were prepared for the primer Set 2 and Probes 1 and primer Set 2 and Probe 2, the probes were evaluated testing the positive plasmid control (PC) and NTC, the probe 2 was chosen for the next step considering it produced a positive band for the positive control and no band for the non-template control.

To evaluate if the Primer Set t and Probe 2 could differentiate the positive control from the wild-type version from spike gene (negative control), master mixes were prepared for Primer Set 2/Probe 2 testing positive control (PC), a triplicate of negative control (NC) based on a 395 nt segment wild-type for del211/214ins (S_211del+214ins_Wildtype) (10^5 copies/µL) (Table 1) and NTC, the results were evaluated using lateral flow strips and gel electrophoresis analysis.

3.3. Synthesis of RNA Standards

3.3.1. Nucleocapsid Gene

The initial RPA primers for the nucleocapsid gene, which were designed to be 32 nucleotides in length, were shortened to 22 nucleotides to be used in PCR. This was done because the optimal primer length for PCR is in the range of 18 to 22 nucleotides, in addition, the T7 promoter sequence was inserted on the 5' of the forward primer, labeled as PCR_T7_N_2F and the reverse primer PCR_T7_N_2R (Table 2). The 2019-nCoV_N_Positive Control (IDT, Coralville, IA, USA) (Catalog#10006625) was amplified using PCR. The master mix was composed of 0.5 µL PrimeSTAR® HS DNA Polymerase enzyme (2.5 U/µL) (Takara, Japan), 10 µL of 5x PrimerSTAR buffer, 4 µL of dNTP Mixture (2.5mM), 1 µL of Primer PCR_T7_N_2F (100 nM), 1 µL of reverse PCR_T7__N_2R (200 nM), 1 µL of plasmid control at $2x10^5$ copies/µL, and 32.5 µL of nuclease-free water. The PCR conditions were as follows: 95°C x 10 Sec [98°C x 10 sec, 55 °C x 55 sec, and 72 °C x 15 sec] x 30 cycles. The amplification products were analyzed using 3% gel electrophoresis and purified using the QIAquick® PCR Purification kit (Qiagen, Hilden, Germany). The DNA concentration was determined using a Qubit®2.0 Fluorimeter (Invitrogen, Waltham, MA, USA).

The amplification products were then concentrated by adding 0.1 volumes of Sodium Acetate (3M) and 2.5 volumes of absolute ethanol. The mixture was incubated on ice for 20 minutes, followed by centrifugation at 15000 RPM at 4°C for 20 minutes. The supernatant was decanted and dried for 5 minutes, after which 200 µL of 75% ethanol was added. Then the mixture was

centrifuged at 15000 RPM at 4°C for 5 minutes. The supernatant was discarded, and the pellet was reconstituted with 25 µL of TE buffer (10 mM Tris·HCl, pH 8.0/1 mM EDTA) (Nippon Gene, Tokyo, Japan). The DNA concentration was determined using a Qubit®2.0 Fluorimeter (Invitrogen, Waltham, MA, USA).

Next, eight µL of PCR amplicon was used for the RNA transcription template using the MEGAshortscriptTM Kit (Ambion, Austin, TX, USA) following the manufacturer's instructions. The RNA was purified using the RNAeasy Minikit (Qiagen, Hilden, Germany), and the DNA was quantified using a Qubit®2.0 Fluorimeter (Invitrogen, Waltham, MA, USA).

As previously described, I calculated the number of RNA copies based on the amount of RNA, the amplicon length, and Avogadro's number[58]. The RNA standards were aliquoted and stored at -80°C.

3.3.2. Spike Gene

The RPA primers previously designed in this study for the partial spike gene originally in 32 nucleotides length were shortened to 22 nt, because PCR requires an optimal primer size around the 18—22 nucleotides. Additionally, the T7 promoter sequence was inserted in the 5' end of the forward primer (Table 2). The DNA positive control for Omicron BA.1 (S_211del+214ins_deleted) was amplified by PCR using the following reaction mix: 0.5 µL of PrimeSTAR® HS DNA Polymerase enzyme (2.5 U/µL) (Takara, Tokyo, Japan), 10 µL of 5x PrimerSTAR buffer, 4 µL of dNTP Mixture (2.5 mM), 1 µL of PCR_T7_214ins_SET2_F (100 nM), 1 µL of reverse PCR_T7_214ins_SET2_R (200 nM), 1 µL of plasmid control (1x108 copies/µL),

and 32.5 µL of nuclease-free water. The PCR conditions were 95°C x 10 Sec [98°C x 10 sec, 55 °C x 55 sec and 72 °C x 15 sec] x 30 cycles. The amplification products were analyzed by a 3% gel electrophoresis and purified using the QIAquick® PCR Purification kit (Qiagen, Hilden, Germany). The DNA concentration was determined using a Qubit®2.0 Fluorimeter (Invitrogen, Waltham, MA, USA).

Next, eight µL of the PCR amplicons were used for the RNA transcription template using the MEGAshortscriptTM Kit (Ambion, Austin, TX, USA) following the manufacturer's recommendations. The RNA was purified using the RNAeasy Minikit (Qiagen, Hilden, Germany) and quantified using a Qubit®2.0 Fluorimeter (Invitrogen, Waltham, MA, USA). The number of copies was calculated as previously described. The RNA standard was aliquoted and stored at -80°C.

3.4. Determination of the Limit of Detection

3.4.1. Nucleocapsid Gene

One-step isothermal SARS-CoV-2 RNA amplification and detection were developed using the TwistAmp Basic RPA Kit (TwistDX, Cambridge, UK), reverse transcriptase Moloney Murine Leukemia Virus enzyme (M-MLV) (Invitrogen, Carlsbad, CA, USA), and endonuclease IV (New England Biolabs, Ipswich, MA, USA). The mixture comprised rehydration buffer (29.5 µL), nuclease-free water (6 µL), forward primer (RPA_N_2F) (360 nM) (Table 2), reverse biotin-labeled primer (RPA_N_2R-Bio) (360 nM), M-MLV (4 U/µL), dithiothreitol (DTT) (2 mM) (Invitrogen), endonuclease IV (0.1 U/µL),

RNAaseOUT^{TM} (0.4 U/µL) (Invitrogen), and RPA_Probe_N1 (40 nM). The mixture was transferred to a microtube containing pellet enzymes provided with the RPA Kit. Magnesium acetate (14 nM) was then carefully applied to the inner part of the tube lid. Finally, 5 µL of an RNA template was added to the mixture, resulting in a final volume of 50 µL. The reaction tube was centrifuged for 5 s, vortexed for 3 s, and centrifuged again. The mixture was incubated at 37 °C for 30 min using a block heater CTU-N (Taitec Co., Ltd., Tokyo, Japan). I performed a gentle hand-mixing and centrifuged the mixture after 5 min of incubation.

To assess the limit of detection of the SARS-CoV-2 (N) assay, I tested 10-fold dilutions of RNA standards with concentrations equivalent to 10^4, 10^3, 10^2, and 1 copies/µL in two independent experiments. The standards consisted of a 166-nucleotide segment of the N gene flanked by the RPA primers of the SARS-CoV-2 (N) RT-RPA-LF. Nuclease-free water was used as NTC. The 6-FITC and biotin-labeled amplicons generated by the SARS-CoV-2 (N) RT-RPA-LF were detected using HybriDetect lateral flow strips (Milenia Biotec, Gieben, Germany). In a tube, 2 µL of RPA amplicon was carefully mixed with 98 µL of assay buffer. The lateral flow strip was then immersed in the buffer, and positive results were considered if a band was confirmed within 5 min, as previously described [59]. In addition, the amplification products were analyzed by a 3% gel electrophoresis.

3.4.2. Spike Gene

One-step isothermal Omicron BA.1 RNA (del211/ins214) amplification and detection was developed preparing a master mix containing rehydration buffer (29.5 µL), nuclease-free water (4.6 µL), forward primer (RPA_214ins_SET2_F) (480 nM) (Table 2), reverse biotin-labeled primer (RPA_214ins_SET2_R_Bio) (480 nM), M-MLV (4 U/µL), DTT (2 mM), endonuclease IV (0.1 U/µL), RNAaseOUT^{TM} (0.4 U/µL), and RPA_214INS_Probe_2 (60 nM) (Table 2) the mixture was transferred to a microtube containing the pellet enzymes provided in the RPA Kit. Magnesium acetate (14 nM) was then carefully applied to the inner part of the tube lid. Finally, 5 µL of an RNA template was added to the mixture, resulting in a final volume of 50 µL. The reaction tube was centrifuged for 5 s, vortexed for 3 s, and centrifuged again. The mixture was incubated at 37 °C for 30 min in a block heater. Soft hand mixing and spin-down were performed after the first five minutes of incubation.

I evaluated the limit of detection of the Omicron BA.1 assay testing 10-fold dilutions of RNA standards with concentrations equivalent to 10^4, 10^3, 10^2, and 1 copies/µL in three independent experiments. The RNA standards corresponded to a 185-nucleotide segment of the S gene containing the (del211/ins214), as previously described. A synthetic segment of 395 bp of the S gene of the (wild-type) flanked by the Omicron BA.1 primer was used as a negative control. Nuclease-free water was used as NTC. The amplicons were analyzed using lateral flow strips. In a tube, 2 µL of RPA amplicon was carefully mixed with 98 µL of assay buffer. The lateral flow strip was then immersed in the buffer, and positive results were considered if a band was confirmed within

5 min, as previously described [59]. In addition, the amplification products were analyzed by a 3% gel electrophoresis.

3.5. Cross-reactivity

To evaluate the cross-reactivity of the SARS-CoV-2 (N) RT-RPA-LF and Omicron BA.1 (S) RT-RPA-LF assays, we tested the standards (ATCC, Manassas, VA, USA), virus isolates, and clinical samples associated with some common human respiratory viruses (Table 3).

3.6. Clinical samples

In this study, I received 454 clinical respiratory samples from two hospitals and three laboratories in Miyagi, Japan, and Peru (Figure 8, Table 3). One hundred eleven nasopharyngeal samples were collected from children with respiratory symptoms before the COVID-19 pandemic. Among 328 SARS-CoV-2-positive samples, 86 were included for the evaluation of SARS-CoV-2 (N) RT-RPA-LF (Figure 9), and 257, including variants of BA.1 (n = 172), BA.2 (n = 15), BA.5 (n = 7), Alpha (n = 15), Delta (n = 15), Gamma (n = 7), Lambda (n = 10), and Mu (n = 1), were tested to evaluate Omicron BA.1 (S) RT-RPA-LF (Figure 10). Sixty-seven pre-pandemic samples were tested in both RT-RPA-LF assays.

SARS-CoV-2 variants were identified based on Sanger sequencing (partial S gene, Table 6) or whole genome sequencing. The SARS-CoV-2 sequences collected in Japan (n = 224) and included in the Omicron BA.1 (S) RT-RPA-LF testing have been submitted to GISAID (Table 8). Also, the genetic sequences from samples collected and previously submitted in Perú (n = 33) were

accessed from GISAD to assess the presence of del211/ins214 and establish the group wildtype and non-BA.1 VOC. The accession numbers of these sequences can be found in Table 8.

The RNA was extracted using QIAmp® Viral RNA Mini Kit (Qiagen, Valencia, CA, USA), MagMAX™ CORE Nucleic Acid Purification Kit (ThermoFisher Scientific, Paisley, UK), Maxwell RSC Total Nucleic Acid Purification Kit (Promega, Madison, WI, USA) and Nucleic Acid Extraction-Purification kit (Sansure Biotech, Changsha, China). The samples were tested for SARS-CoV-2 using real-time RT-PCR [5,53] and preserved at -80 °C until further utilization.

3.6.1. Ethical Statement

The research project was reviewed and approved by the Institutional Ethics Committee of the Graduate School of Medicine, Tohoku University (2020-1-333, N-19577) and Peruvian Cayetano Heredia University (SIDISI:212025 and 205559).

3.7. Diagnostic evaluation of SARS-CoV-2 (N) RT-RPA-LF

A total of 190 clinical samples were tested to evaluate the SARS-CoV-2 (N) RT-RPA-LF assay. The samples were divided into a "positive group" (n=86), consisting of samples that tested positive using SARS-CoV-2 RT-qPCR and a "negative group" (n=104), consisting of nasopharyngeal swabs samples collected before the COVID-19 pandemic (Figure 9). The positive group was stratified by different viral load categories according to quantitative real-time PCR results as follows: high > 9015 copies/µL (Cq<24.9), moderate 9015—

385 copies/µL (Cq 25—29.9), low 385—16 copies/µL (Cq 30—34.9) and very low <16 copies/µL (Cq 35—40) following similar categorization established in previous studies [52,60]. The sensitivity on clinical samples was calculated independently for each category and I performed the evaluation of RT-RPA-LF blinded to the SARS-CoV-2 real-time RT-PCR results of the samples. *In vitro* transcribed RNA standard (10^5 copies/µL) was utilized as a positive control, and nuclease-free water was utilized as NTC in all the experiments. The test results were annotated in Table 5a.

3.8. Diagnostic evaluation of the Omicron BA.1(S) RT-RPA-LF

Similarly, 331 clinical samples were tested to evaluate the Omicron BA.1 (S) RT-RPA-LF assay. Based on Sanger or NGS results, I created a "positive group" (n=172) consisting of samples confirmed to be Omicron BA.1. Samples were selected by Cq level categories as described above (Figure 10). I established two "negative groups": the wild-type+non-BA.1 VOC group (n=85), consisting of specimens confirmed as wild-type and VOCs other than BA.1, and pre-COVID-19 specimens (n=74). The procedure was carried out blinded, as explained above. Transcribed RNA standard containing the del211/ins214 (10^5 copies/µL) was used as a positive control, and a plasmid containing the wild-type for del211/ins214 (10^5 copies/µL) was used as a negative control. Nuclease-free water was utilized as NTC. The results for Omicron BA.1 (S) RT-RPA-LF were annotated in Table 5b.

4. Results

4.1. Primer design

For the molecular detection of the SARS-CoV-2 Nucleocapsid gene, two RPA primer sets and one probe were designed. Moreover, three RPA primers and two probes were designed for the SARS-CoV-2 spike region, covering the del211 and ins214 (Table 2).

4.2. Primer selection

4.2.1. Nucleocapsid Gene

The primer Sets RPA_N1 and RPA_N2 showed a band under gel electrophoresis analysis for the positive plasmid control, however, RPA_N2 showed a significantly more intense band (Figure 4) so I chose it for the next development process.

4.2.2. Spike Gene

The primers Set 2 and Set 3 produced an amplification band under gel electrophoresis analysis (Figure 5a), however, the primer Set 2 was chosen for the next developing process since it produced a slightly more intense band under visual qualitative analysis compared to primer Set 3, no band was observed for NTC. The primer Set 2 showed a limit of detection of 10 copies/µL testing the positive control (Figure 5b). Probe 1 and Probe 2 showed a test line in the positive control for the lateral strip however, only Probe 2 showed to work properly showing the absence of a band on the lateral flow for the NTC (Figure 5c). The presence of amplicon on the positive control and absence of amplicon

on the NTC was confirmed using gel electrophoresis analysis (Figure 5d). Probe 2 was chosen for the next development step.

The primer Set 2 and Probe 2 proved to discern the positive control containing the del211 and ins214 from the negative control containing the wild-type version of the del211 and ins214, showing band for the lateral flow for the positive control and band at any of the triplicates of the negative control, also no bad was observed on the NTC (Figure 5e). The proper function of the primer and probe mechanism was confirmed by gel electrophoresis analysis, observing amplification bands in the positive and negative controls. The presence of bands in the negative controls is explained as a result of correct annealing of the primers to the partial segment of the spike gene of the SARS-CoV-2 (Figure 5f), only Probe 2 was designed to discern a segment containing del211 and ins214 from a wild-type. Finally, the combination of the Primer Set 2 and probe 2 was selected for the evaluation of clinical samples.

4.3. Determination of the Limit of Detection

4.3.1. Nucleocapsid Gene

The SARS-CoV-2 (N) RT-RPA-LF showed a limit of detection of 10 copies/µL (RNA standards) (Figure 6a, b).

4.3.2. Spike Gene

The Omicron BA.1 (S) RT-RPA-LF showed a limit of detection of 10 copies/µL (RNA standards) (Figure 6c, d).

4.4. Cross-reactivity

4.4.1. Nucleocapsid Gene

The SARS-CoV-2 (N) RT-RPA-LF did not show cross-reactivity against some of the most common human respiratory viruses, including human metapneumovirus, influenza A (H1N1)pdm09, respiratory syncytial virus, human parainfluenza virus type 2, human parainfluenza virus type 4, human adenovirus, human parainfluenza virus type 1, human parainfluenza virus type 3, influenza B virus, influenza C virus, severe acute respiratory syndrome coronavirus, and middle east respiratory syndrome coronavirus (Figure 7a), human coronavirus 229E and human coronavirus OC43 (Figure 7b, Table 4).

4.4.2. Spike Gene

The Omicron BA.1 (S) RT-RPA-LF did not showed cross-reactivity testing pre-COVID-19 coronaviruses 229E, OC43, NL63, and HKU1, (Figure 7c, d), Alpha and Delta VOCs (Figure 7e, f, Table 4).

4.5. Diagnostic evaluation of SARS-CoV-2 (N) RT-RPA-LF

The sensitivity against the real-time RT-PCR-positive clinical samples varied according to the viral load categories as follows: 100.0% (95% CI: 98.7.1–100.0) for samples with high viral load, 100.0% (95% CI: 97.1–100.0) for those with moderate viral load, 83% (95% CI: 63.3–100.0) for those with low viral load, and 14.3% (95% CI: 0–47.4) for those with very low viral load (Figure 11a, Table 5a). We observed six false negatives under the very low viral load category, of which three resulted below the limit of detection of 10 copies/µL, while others showed 19.55, 23.25, and 53.5 copies/µL. The specificity against

pre-COVID-19 samples was 100% (95% CI: 96.6–100). The detection time from reaction incubation to detection was approximately 35 min.

4.6. Diagnostic evaluation of the Omicron BA.1 (S) RT-RPA-LF

The sensitivity varied according to the real-time RT-PCR Cq categories as follows: 94.9% (95% CI: 90.3–99.8) for high viral load, 78% (95% CI: 65.5–90.5, CI = 95%) for moderate viral load, 23.8% (95% CI: 3.21–44) for low viral load, and 0% for very low viral load (Figure 7b, Table 5b). We observed three false negatives in the very low viral load category, of which two showed a viral load below the limit of detection of 10 copies/µL, and one sample was close to the limit of detection, showing 16.3 copies/µL. The specificities against the wild-type and non-BA.1 VOC samples and pre-COVID-19 samples were 96.5% (90.1–100, CI = 95%) and 95.9% (95% CI: 88.7–98.9), respectively.

The Omicron BA.1 (S) RT-RPA-LF testing yielded six false-positive results, of which three resulted from the negative group of wild-type +non-BA.1 VOC and the other three from the pre-COVID-19 group. We confirmed that there were no del211/ins214 mutations in the sequences from the samples with false-positive results in the wild-type+non-BA.1 VOC group. Three re-tested samples from the six false-positive samples yielded negative results. Therefore, we considered that the false positives occurred mainly due to technical issues during sample loading or amplicon dilution before lateral flow strips.

Among the 172 Omicron BA.1-positive samples tested, I could not assess the presence or absence of del211/ins214 in five sequences; however, those samples were included in the sensitivity analysis because they were able to be

classified as BA.1 lineage using the Pangolin COVID-19 Lineage Assigner. The viral load for those samples was 2.3, 19.1, 31.5, 60.4, and 1545.2 copies/µL. The frequencies of del211 and ins214 in sequences from 167 Omicron BA.1-positive samples, tested by Omicron BA.1 (S) RT-RPA-LF excluding those five samples without the sequences, were 100% (167/167) and 99.4% (164/167), respectively. The result of the sample missing the ins214 was positive by Omicron BA.1 (S) RT-RPA-LF. None of the 85 samples in the “wild-type and non-BA.1 VOC” group had del211 or ins214.

5. Discussion

In this study, I developed and evaluated two RPA assays for the detection of the SARS-CoV-2 partial N gene and Omicron BA.1 variant-specific deletion-insertion mutations in the S gene. The detection limit using the RNA standard (10 copies/µL) was similar to [61] or slightly higher than that reported in other SARS-CoV-2 RT-RPA studies [62,63]. In addition, the detection limit was lower than that of other isothermal amplification methods developed for SARS-CoV-2, such as the 100 RNA copies for LAMP [64,65]. However, the RPA assays had slightly lower sensitivity than that found using real-time RT-PCR, reported by the Centers for Disease Control and Prevention, World Health Organization[66], and the Japanese National Institute for Infectious Diseases, whose detection limit is reported as 1 copy/µL [53].

Several previous studies have evaluated SARS-CoV-2 RT-RPA in clinical samples and reported sensitivities ranging from 65% to 100% and specificities ranging from 77% to 100% [62,63,67–70]. However, among these studies, only three

included > 50 SARS-CoV-2-positive clinical samples. Gosh et al. evaluated the sensitivity of different viral load categories in RT-PCR-positive samples in 76 positive clinical samples [69]. The sensitivities of RT-RPA-N for samples with Cq levels of 0–30, 31–35, and 36–40 were 97.4%, 71.4%, and 12.5%, respectively. Similarly, this study showed the high sensitivity of the SARS-CoV-2 (N) RT-RPA-LF assay in clinical samples with relatively high and moderate viral loads (both 100%). Another study reported a high sensitivity of 98.7% using RT-RPA-targeting N genes in 78 positive samples [68].

Although my results and those of others showed decreased sensitivity in samples with moderate and low viral loads, my two RT-RPA assays seemed to have better sensitivity than Ag-RDT [51,52] in low (N: 83%, BA.1: 24% vs. Ag: 0–14%) to moderate (N: 100%, BA.1: 78% vs. Ag: 42–86%) viral load samples (Table 7). Compared with the sensitivity of the LAMP [64], my assay also showed higher sensitivity in the limited number of low-viral load samples (N: 83.3% vs. 20%) whereas, the BA.1 assay showed comparable sensitivity (24%) to the LAMP.

The higher sensitivity of RPA compared to LAMP in clinical samples with low viral load may be explained in part by the greater efficiency of RPA in amplifying a single target gene, as opposed to the six different target genes amplified by LAMP[23]. This difference in sensitivity may be more evident in clinical samples with low viral load.

Another explanation relies on the colorimetric detection method commonly used by LAMP, that have been reported to obtain false negatives in clinical

samples due to the ambiguity of distinguishing positives from negatives by color changes, especially in clinical samples under low viral loads [71].

In other studies, the RT-RPA assay was combined with clustered regularly interspaced short palindromic repeats (CRISPR)/CRISPR-associated proteins (Cas) to improve sensitivity [72,73]. A study of CRISPR/Cas12a showed similar sensitivity as that observed in this study, and the others showed similar or slightly lower sensitivities using CRISPR/Cas12b (40 copies/µL) or CRISPR/Cas9 assays (8 copies/µL) [73], compared to my study. Only a few studies have applied RT-RPA with CRISPR to a large number of clinical samples. One study that evaluated 53 positives and 111 negatives samples showed a high sensitivity of 96.3% and a specificity of 100% [72]. Another relatively small study with 36 positive and 12 negative samples reported a sensitivity of 93.8% [35].

In this study, I did not utilize CRISPR, which usually requires a two-step system and additional incubation time. Instead, I developed an alternative, simple, and straightforward system that prioritized the time for testing. To the best of my knowledge, no study has reported the sensitivity of RT-RPA with CRISPR/Cas according to viral load levels. This may be feasible, particularly for samples with low viral loads.

Even though both the SARS-CoV-2 (N) and the Omicron BA.1 (S) assays had the same limit of detection (10 copies/µL), the SARS-CoV-2 (N) assay showed higher sensitivity than the Omicron BA.1 (S) assay in clinical samples, especially for moderate to very low viral loads. This difference in sensitivity may

be due to multiple factors, including the potential degradation of RNA due to repeated freeze-thaw cycles [74], different periods of sample preservation [75], the exclusive use of the N gene instead of the S gene for viral RNA detection and its quantification using real-time PCR, as well as a possible difference in the expression rate between the N and S genes.

RNA degradation as a consequence of freeze-thaw cycles is explained due to the activity of RNAases released by disrupted lysosomes in preserved tissues or cleave pressure by ice crystals on mRNA molecules [76]. For instance, during the evaluation of the positive group of Omicron BA.1 (S), the samples underwent up to three thawing cycles because of the procedures of real-time PCR, cDNA synthesis for sequencing, and RPA testing whereas the samples used for the evaluation of the SARS-CoV-2 (N) test only experienced two thawing steps. Additionally, the average time difference from the SARS-CoV-2 real-time PCR to RPA for the positive samples was longer for the Omicron BA.1 test than the SARS-CoV-2 test (4.5 vs. 2.9 months).

To quantify the viral load in the clinical samples, only the SARS-CoV-2 (N) gene real-time PCR assay was employed and not the S gene. However, it is important to note that the expression levels of subgenomic RNA of the N gene and the S gene in SARS-CoV-2 may not be directly comparable. Previous studies in Coronaviruses have indicated that the subgenomic RNA expression of the N gene is 3—10 times higher during 12 hours post-infection[7,77]. Hence, a higher expression of subgenomic RNA of the N gene compared to the S gene

may explain the higher sensitivity of the SARS-CoV-2 (N) test compared to the Omicron (S) test in clinical samples.

Deletions and insertions have been used as molecular markers for the detection and characterization of viruses other than SARS-CoV-2 [78,79]. I selected del211/ins214 as a molecular marker since I found highly prevalent in Omicron BA.1 during the primer design analysis. Deletions and insertions are significant sources of genetic diversification and can induce a significant impact on the properties and evolution of proteins [80]. It is also known to facilitate Alpha and Omicron viral entry mediating spike stability and immune evasion [81]. Also, it shows an association in drug resistance for HIV-1 mediating viral reverse-transcriptase fitness [82].

Although Omicron BA.1 is not circulating anymore, I addressed the applicability of an assay to detect a SARS-CoV-2 variant containing deletions/insertions. The test design reported in this study may be useful in future applications for the detection of SARS-CoV-2 VOC using deletions/insertions as molecular markers.

In this study, I developed a one-step RT-RPA-LF system. This system utilizes a reverse transcriptase enzyme to enable complementary DNA synthesis (cDNA), along with a probe labeled with FITC and a reverse primer labeled with Biotin. Additionally, it incorporates an endonuclease IV and utilizes commercially available lateral flow strips (LF) designed for the detection of DNA amplicons labeled with FITC and Biotin. The developed system allows for the detection of SARS-CoV-2 and Omicron BA.1 in less than 35 minutes. This

approach offers a faster and straightforward alternative to previously reported methods targeting other mutations in SARS-CoV-2 VOC [35,36].

I designed a probe to bind to the remaining ends of the deletion/insertion and detect the mutation as a positive result, which is different from other PCR methods that give negative results for deletion detection [83]. One sample with del211 but without ins214 was also positive, possibly because the probe annealed to a portion of the remaining del211 ends. Detecting specific deletions seems useful; however, these mutations may be shared with new variants in the future. Therefore, genomic monitoring of the sequence is necessary. For example, Omicron XBB.1.5, currently circulating in the United States and other countries, shares most of its spike mutations with BA.2, including a deletion mutation in del144 [84], which was previously observed in Alpha and other variants of interest.

The cost per sample for the RT-RPA-LF was 3,000 Japanese yen (JPY), which is three times more expensive than real-time PCR (1,100 JPY) and also more expensive than rapid antigen tests (800 JPY). These costs include the price of the RNA extraction kit in both cases. However, part of the cost difference may be because of the additional importation or supplier costs due to the low level of distribution in Japan.

Regarding the test development time of RT-RPA-LF, it is estimated to take around two weeks, if a panel is prepared of clinical samples properly characterized as positive and negative controls. This relatively short development period would be useful in scenarios where a rapid response is needed to develop molecular tests for new variants of SARS-CoV-2 or other emerging pathogens.

My study has limitations. First, clinical samples were not analyzed at the same institution using real-time RT-PCR parallel to RT-RPA-LF; therefore, the viral load was lower than the values tested at each institution. Because of RNA degradation due to time or unfreezing, some misclassification of viral load categories may have occurred. Second, the positive sample selection for Omicron BA.1 (S) RT-RPA-LF was limited to samples whose sequences were available by Sanger sequencing or NGS. Mutation-specific real-time RT-PCR, which is a highly sensitive method, allows the addition of a high number of samples with low viral loads. Third, the limited number of samples in the low and very low virus categories resulted in a wide range of 95% CI for sensitivity. Finally, RNA samples obtained from children during the pre-COVID-19 period and other VOCs were used as negative controls. Specificity was not evaluated for samples collected from populations with similar backgrounds and periods.

The RT-RPA-LF system still has some disadvantages for implementation in resource-limited settings. First, the system requires RNA extraction from RNA viruses. Therefore, additional laboratories, equipment, and time are required. Secondly, the lateral flow assay has a higher risk of contamination than the

single-tube assay, which uses coloring techniques. The need to open the reaction tube after amplification to perform lateral flow detection has been highlighted as an important source of cross-contamination, owing to amplicon aerosolization [85].

Therefore, to utilize this sensitive detection method of specific deletion-insertion mutation in SARS-CoV-2 VOC or other RNA virus pathogens in the future, further studies may adapt the instrument-free and rapid nucleic acid extraction methods and/or single-tube systems.

6. Conclusions

In this study I developed two rapid molecular tests for the detection of SARS-CoV-2 nucleocapsid gene (N) and variant-specific Omicron BA.1. Both methods showed high sensitivity and specificity in clinical samples. Further research is needed for the development and adaptation of the instrument-free RNA isolation method which should allow the application of this test in point-of-care or low-resource settings.

7. List of abbreviations

6-FITC	6- fluorescein isothiocyanate
Ag-RDT	Antigen Rapid detection test
CD	Connector domain
cDNA	Complementary DNA
CH	Central helix
COVID-19	Coronavirus disease 2019
Cq	Cycle quantification
CRISPR	Clustered regularly interspaced short palindromic repeats
FCS	Furin-cleave site
FP	Fusion peptide
GISAID	Global Initiative on Sharing All Influenza Data
hACE2	Angiotensin Converting Enzyme 2
HR1	Heptad repeat 1
NGS	Next-generation sequencing
NTD	N-terminal domain
PCR	Polymerase Chain Reaction
RBD	Receptor binding domain
RT-LAMP	Reverse transcription loop-mediated isothermal amplification
RT-RPA	Reverse transcription recombinase polymerase amplification
SARS-CoV-2	severe acute respiratory syndrome coronavirus 2
SSB	Single-stranded DNA binding proteins
TMPRSS2	Transmembrane serine protease 2
VOC	Variant of concern

8. Figures

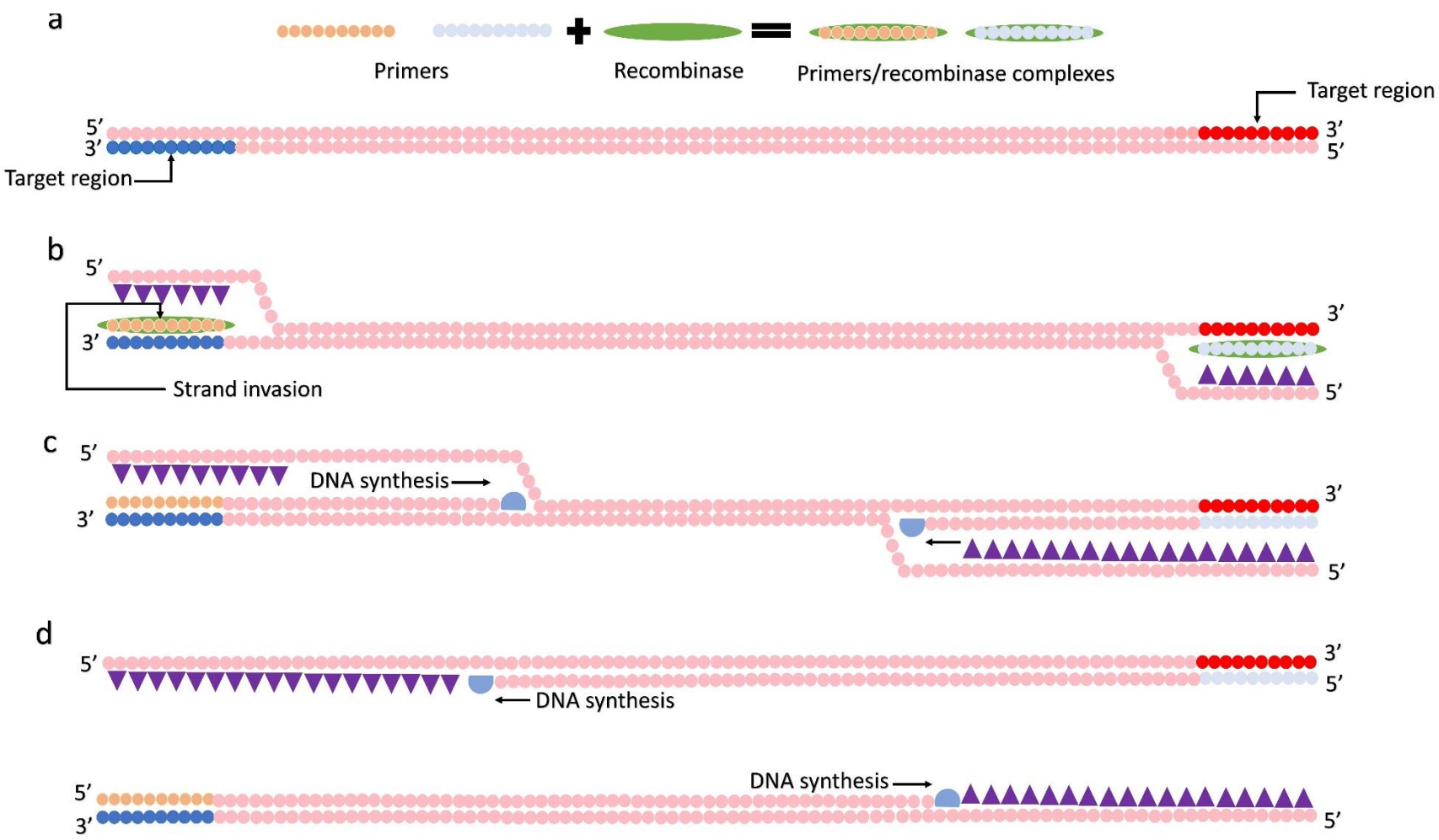
a
Primers
Recombinase
Primers/recombinase complexes
Target region
5′
3′
3′
5′
Target region
b
5′
3′
3′
Strand invasion
5′
c
5′
DNA synthesis
3′
3′
5′
d
5′
3′
5′
DNA synthesis
DNA synthesis
5′
3′
5′

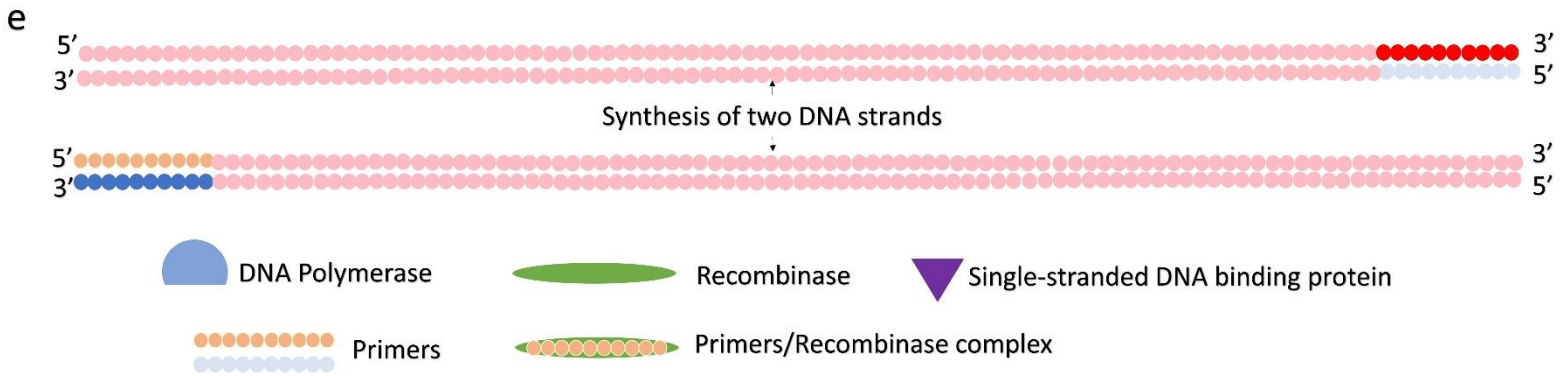

Figure 1. Principle of recombinase polymerase amplification (RPA). **(a)** The RPA primers and Recombinase proteins combine to form a nucleoprotein complex. **(b)** The nucleoprotein complex anneals at the target region sequence, the complementary strand is displaced forming a Loop, and the loop structure is stabilized by single-stranded DNA binding proteins (SSB). **(c)** The DNA polymerase synthetizes DNA from 5' to '3 direction. **(d)** The parental strand separates as DNA synthesis continues. **(e)** Two new DNA strands are synthesized.

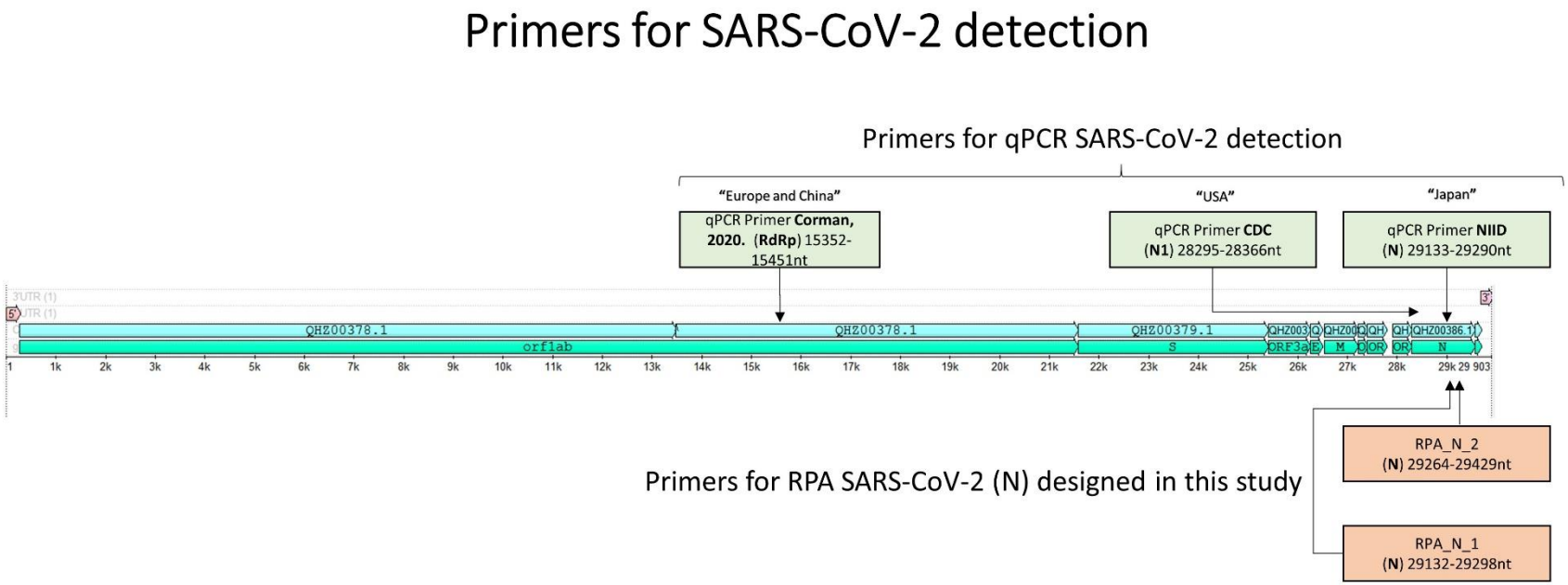

Figure 2. Primer design for SARS-CoV-2 nucleocapsid gene (N).

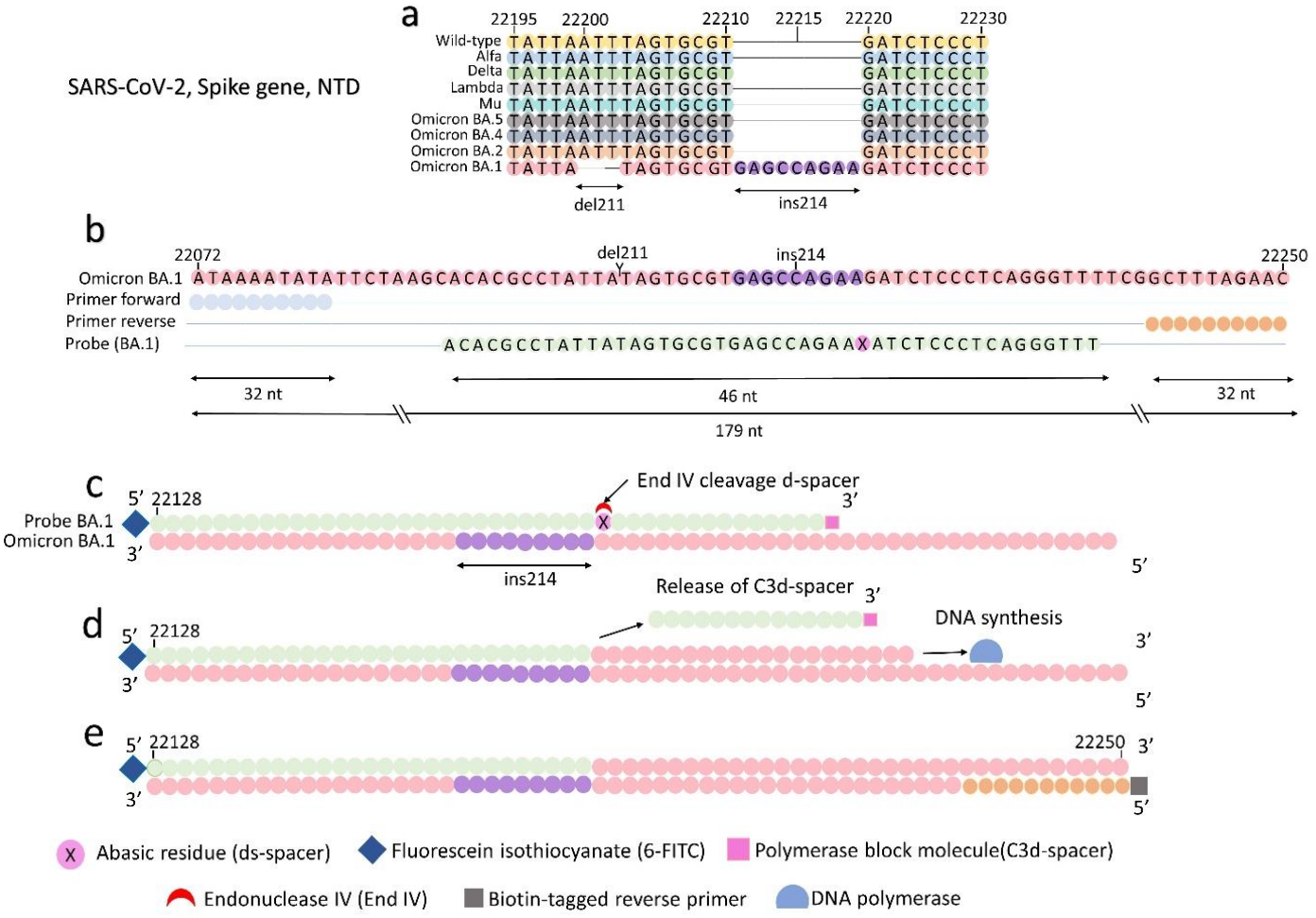
SARS-CoV-2, Spike gene, NTD
a
22195
22200
22210
22215
22220
22230
Wild-type TATTAATTTAGTGCGT GATCTCCCT
Alfa TATTAATTTAGTGCGT GATCTCCCT
Delta TATTAATTTAGTGCGT GATCTCCCT
Lambda TATTAATTTAGTGCGT GATCTCCCT
Mu TATTAATTTAGTGCGT GATCTCCCT
Omicron BA.5 TATTAATTTAGTGCGT GATCTCCCT
Omicron BA.4 TATTAATTTAGTGCGT GATCTCCCT
Omicron BA.2 TATTAATTTAGTGCGT GATCTCCCT
Omicron BA.1 TATTA TAGTGCGTGAGCCAGAA GATCTCCCT
del211
ins214
b
22072
del211
ins214
22250
Omicron BA.1 ATAAAATATATTCTAAGCACACGCCTATTATAGTGCGTGAGCCAGAAGATCTCCCTCAGGGTTTTCGGCTTTAGAAC
Primer forward
Primer reverse
Probe (BA.1) ACACGCCTATTATAGTGCGTGAGCCAGAAXATCTCCCTCAGGGTTT
32 nt
46 nt
32 nt
179 nt
c
5′ 22128
End IV cleavage d-spacer
3′
Probe BA.1
Omicron BA.1
X
3′
5′
ins214
Release of C3d-spacer
3′
d
5′ 22128
DNA synthesis
3′
3′
5′
e
5′ 22128
22250 3′
3′
5′
X Abasic residue (ds-spacer)
Fluorescein isothiocyanate (6-FITC)
Polymerase block molecule(C3d-spacer)
Endonuclease IV (End IV)
Biotin-tagged reverse primer
DNA polymerase

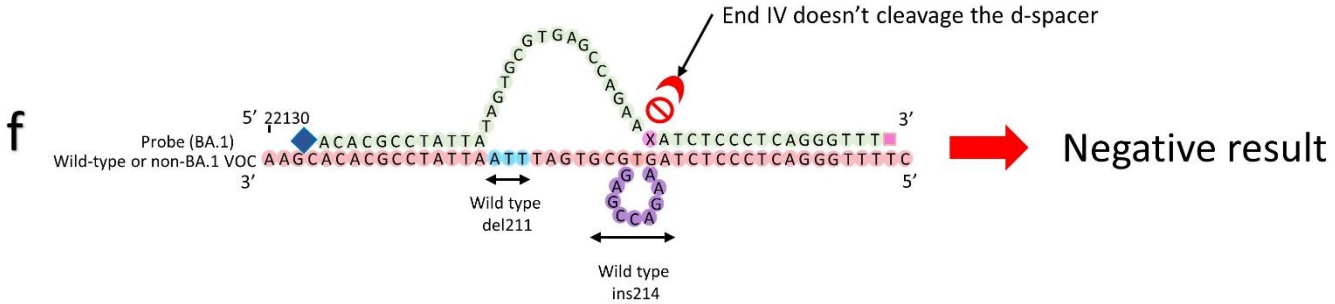
f
End IV doesn't cleavage the d-spacer
5′ 22130
Probe (BA.1)
Wild-type or non-BA.1 VOC
3′
5′
Wild type
del211
Wild type
ins214
Negative result

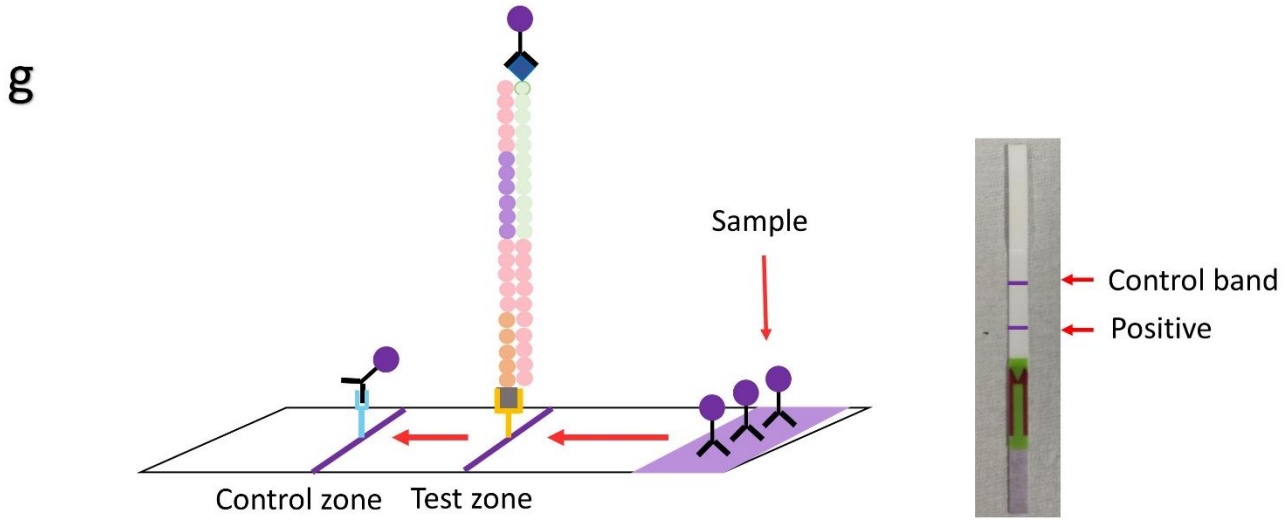
g
Sample
Control band
Positive
Control zone
Test zone

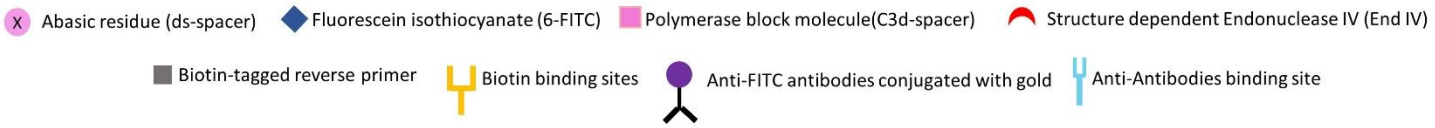
Abasic residue (ds-spacer)
Fluorescein isothiocyanate (6-FITC)
Polymerase block molecule(C3d-spacer)
Structure dependent Endonuclease IV (End IV)
Biotin-tagged reverse primer
Biotin binding sites
Anti-FITC antibodies conjugated with gold
Anti-Antibodies binding site

Figure 3. Principle for Omicron BA.1 (S) RT-RPA-LF. **(a)** representation of the del211/ins214 located in the N-terminal domain (NTD), spike gene, Omicron BA.1. **(b)** RPA primers amplify a 179bp segment, and a 46 nt long probe anneals a segment along the del211/ins214. **(c)** endonuclease IV specifically cleaves the abasic residue (d-spacer) only after alignment of probe and del211/ins214. **(d)** The polymerase block molecule (C3-spacer) is released from the 3‘ probe. The DNA polymerase incorporates nucleotides from 5' to 3'. **(e)** a 179 bp amplicon is synthesized containing a 6-FITC tag at 5'end and a Biotin at 3'.**(f)** a partial or no binding of probe and template won’t allow end IV cleave the abasic residue, as a consequence no double tagged amplicon will be generated producing a negative result. **(g)**The RPA amplicon tagged with FITC and Biotin can be detected by the universal lateral flow strips specific for 6-FITC /Biotin molecules.

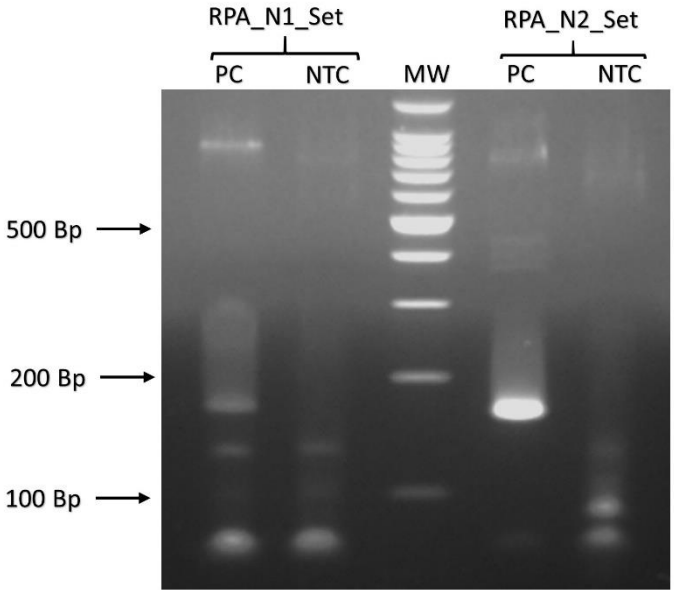

Figure 4. Primer test for the SARS-CoV-2 (N) RT-RPA-LF. The primer set RPA_N2_Set showed a more intense band in the positive control compared to the set RPA_N1_Set. The set RPA_N2_Set was selected for the limit of detection test. MW: Molecular weight marker. Bp: Base pairs. PC: Positive control, CDC The 2019-nCoVN_Positive Control 10^5 copies/µL. NC: Negative control, NTC: Non-template control, nuclease-free water.

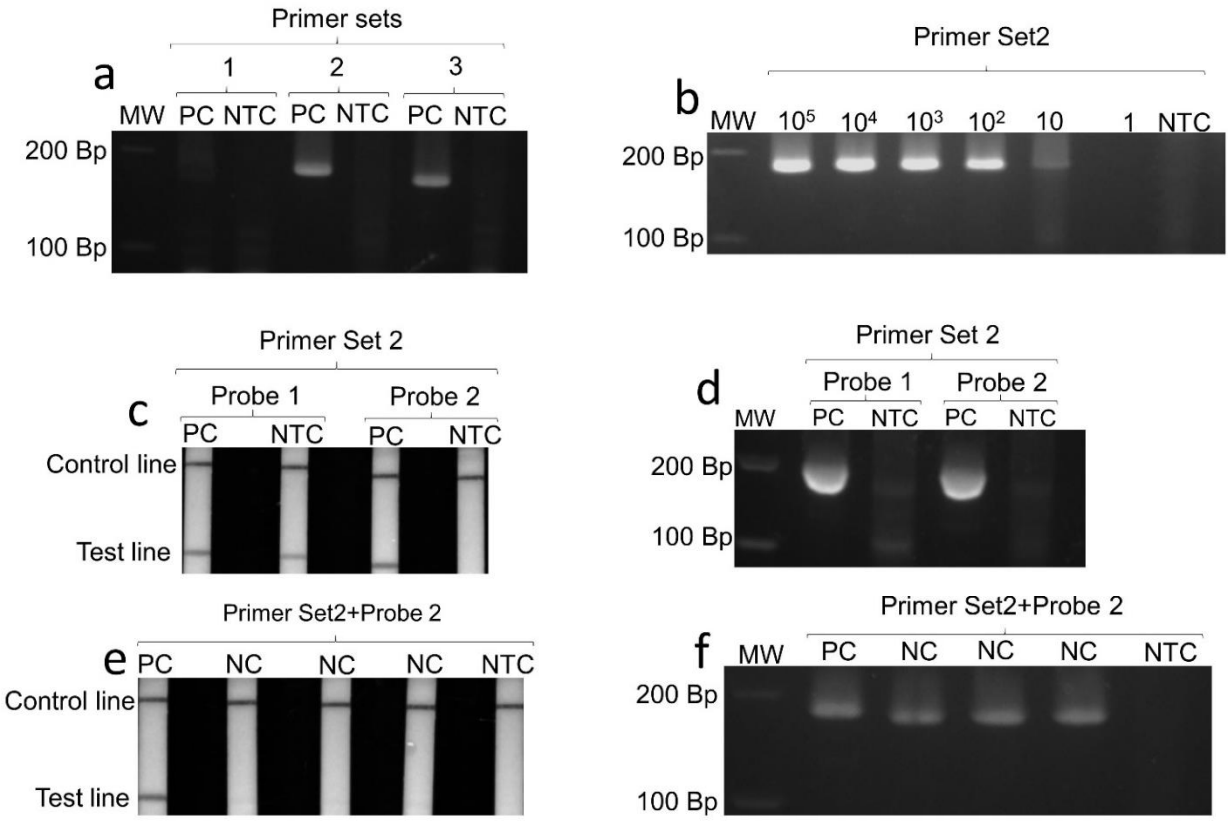

Figure 5. Primer and probe evaluation for the Omicron BA.1 (S) RT-RPA-LF. **(a)** RPA primers evaluation, amplification bands are confirmed on positive control (PC) for primers Set 2 and Set 3, **(b)** gel electrophoresis shows a detection limit of 10 copies/µL (plasmid control) for primer Set 2, **(c)** the combination of primer Set 2 and Probe 2 produced a band on PC. No band was observed for the NTC, and **(d)** gel electrophoresis confirms amplification bands for both probes 1 and 2 at the PC, but no bands were detected at the NTC. MW: Molecular weight marker. Bp: Base pairs. PC: Positive control, del211/ins214 plasmid control 10^5 copies/µL. NC: Negative control, wildtype for del211/214ins plasmid control 10^5 copies/µL. NTC: Non-template control, nuclease-free water.

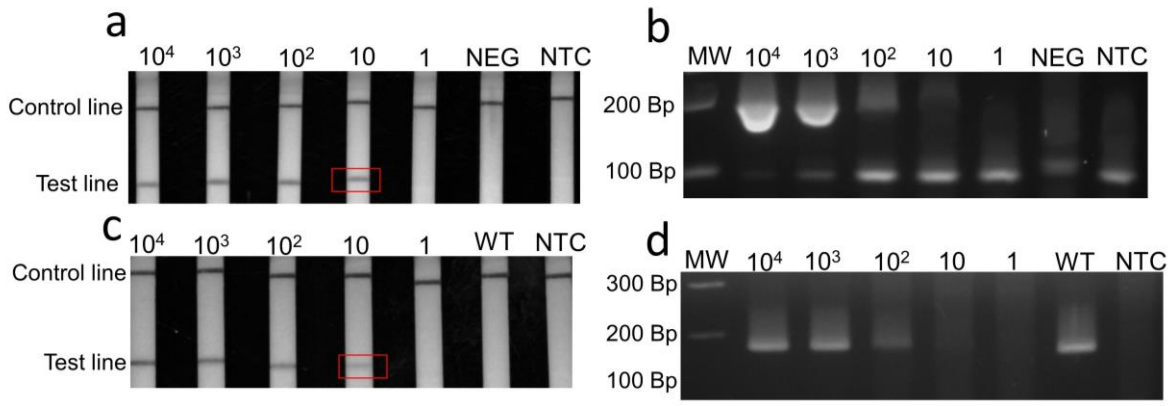

Figure 6. The detection limit of SARS-CoV-2 (N) RT-RPA-LF and Omicron BA.1 (S) RT-RPA-LF based on RNA standards **(a), (b),** SARS-CoV-2 (N) RT-RPA-LF showed a detection limit up to 10 copies/µL of RNA standards, **(c), (d)** The Omicron BA.1 (S) RT-RPA-LF showed a detection limit of 10 copies/µL of RNA standards. WT: wild-type S gene (10^4 Copies/µL). NEG: negative control, human DNA. NTC: non-template control, nuclease-free water. MW: molecular weight marker. Bp: base pairs.

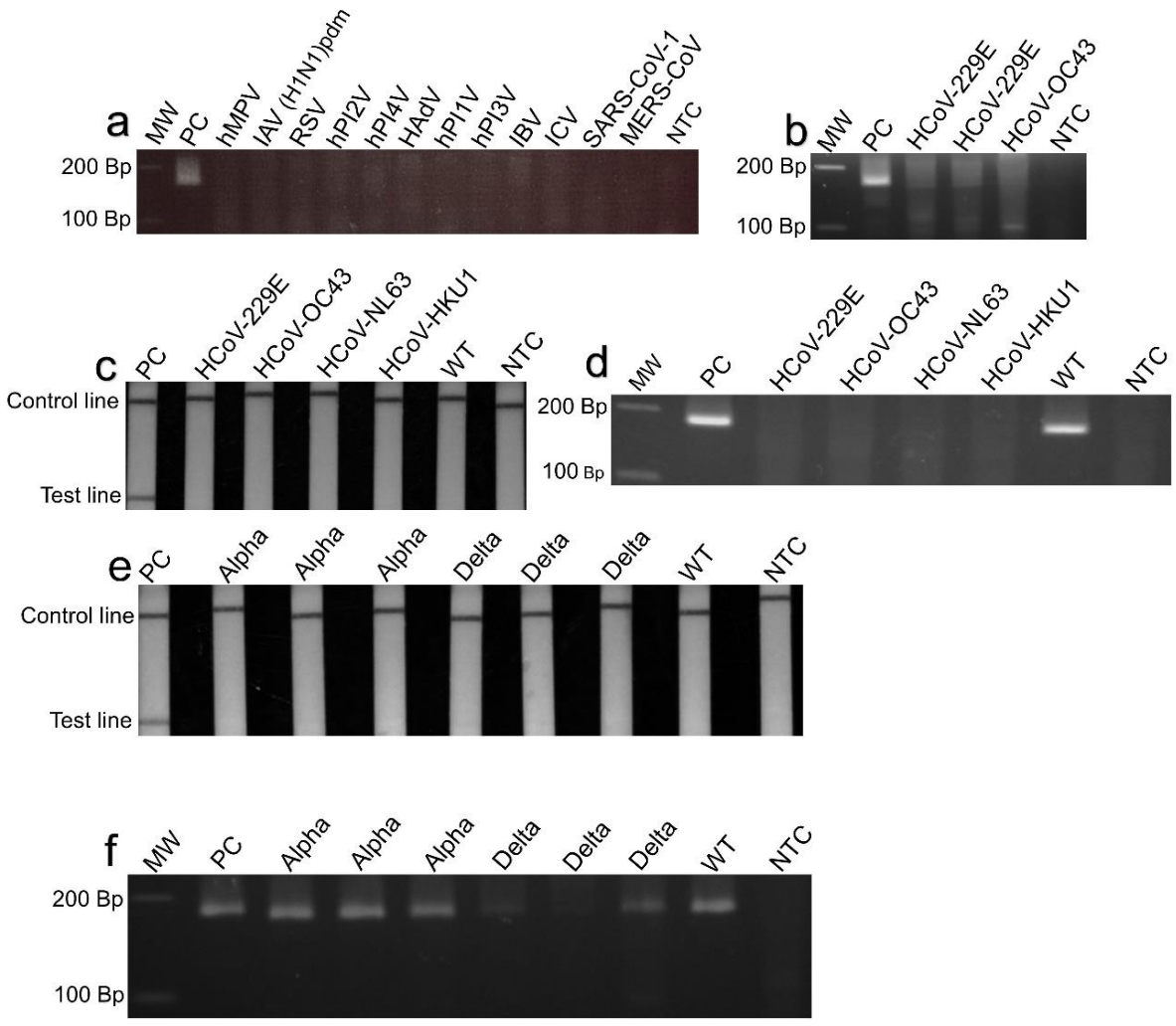

Figure 7. Cross-reactivity of SARS-CoV-2 (N) RT-RPA-LF tested against nucleic acid samples from common respiratory pathogens. **(a)** no cross-reactivity was observed for the SARS-CoV-2 (N) RT-RPA-LF testing human metapneumovirus (hMPV), influenza A (H1N1)pdm09 (IAV H1N1-pdm), respiratory syncytial virus (RSV), human parainfluenza virus type 2 (hPI2V), human parainfluenza virus type 4 (hPI4V), human adenovirus (HAdV), human parainfluenza virus type 1 (hPI1V), human parainfluenza virus type 3 (hPI3V),

influenza B virus (IBV), influenza C virus (ICV), severe acute respiratory syndrome coronavirus (SARS-CoV-1), and middle east respiratory syndrome coronavirus (MERS-CoV), **(b)** no cross-reactivity was observed testing human coronavirus 229E (HCoV-229E) and human coronavirus OC43 (HCoV-OC43), **(c)** No cross-reactivity was observed for the Omicron BA.1 (S) RT-RPA-LF testing pre-COVID-19 coronaviruses 229E (HCoV-229E), OC43 (HCoV-OC43), NL63 (HCoV-NL63), and HKU1 (HCoV-HKU1), **(e),(f),** No cross-reactivity was observed testing Alpha and Delta VOCS. MW: molecular weight. Bp: base pairs. WT: wild-type S gene (10^4 Copies/µL). NTC: non-template control, nuclease-free water.

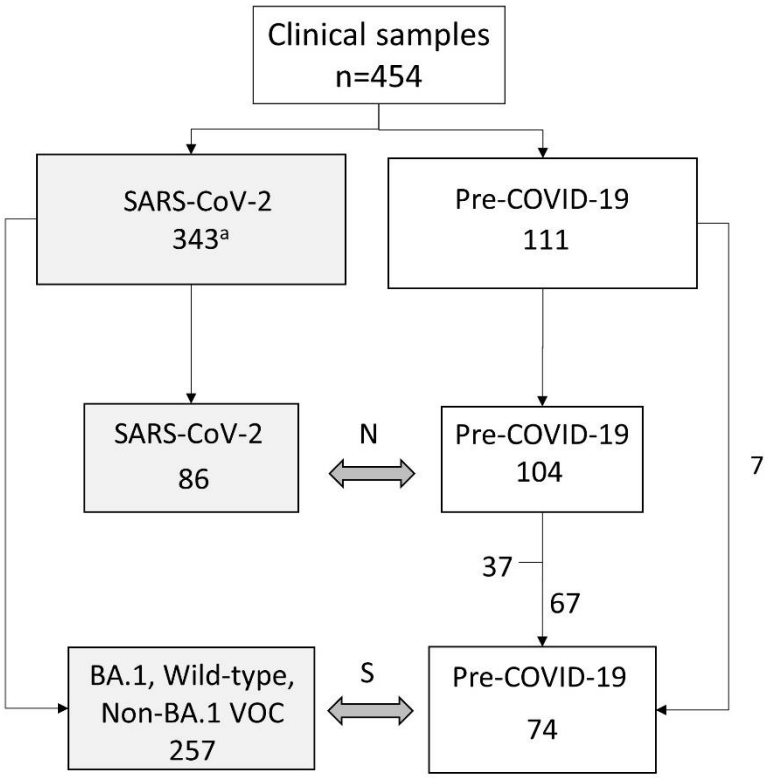

Figure 8. Study design diagram. N: SARS-CoV-2 (N) RT-RPA-LF, S: Omicron BA.1 (S) RPA-LF, VOC: variant of concern. Pre-COVID19: Clinical samples collected before the COVID-19. [a.]The sample numbers by institutions are described in Table 3.

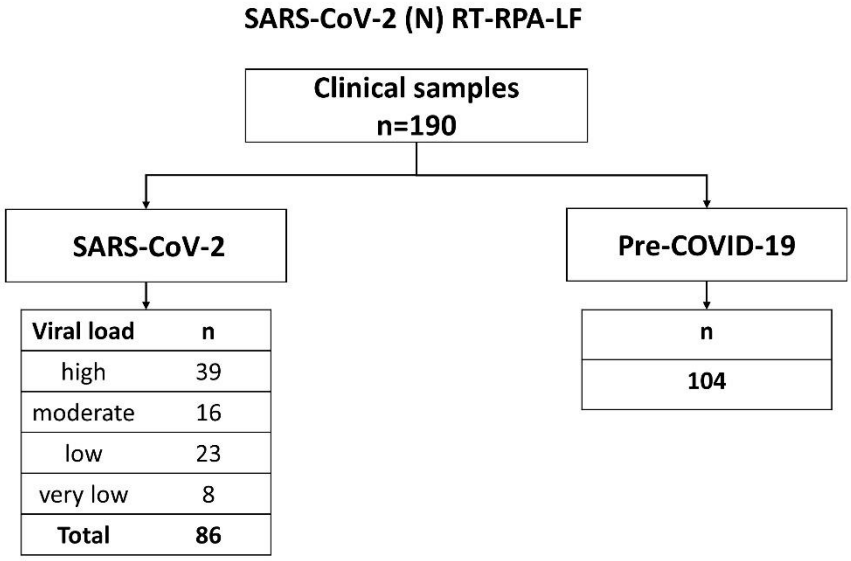

Figure 9. Flow chart of diagnostic evaluation for SARS-CoV-2 (N) RT-RPA-LF

SARS-CoV-2: Clinical samples positive to SARS-CoV-2 by real-time PCR. Pre-COVID19: Clinical samples collected before the COVID-19. The viral loads were stratified as; Hight viral load: > 9777.3 copies/µL, moderate viral load: 503.5—9777.3 copies/µL, low viral load: 25.8—503.4 to copies/µL and very low viral load: < 25.8 copy/µL.

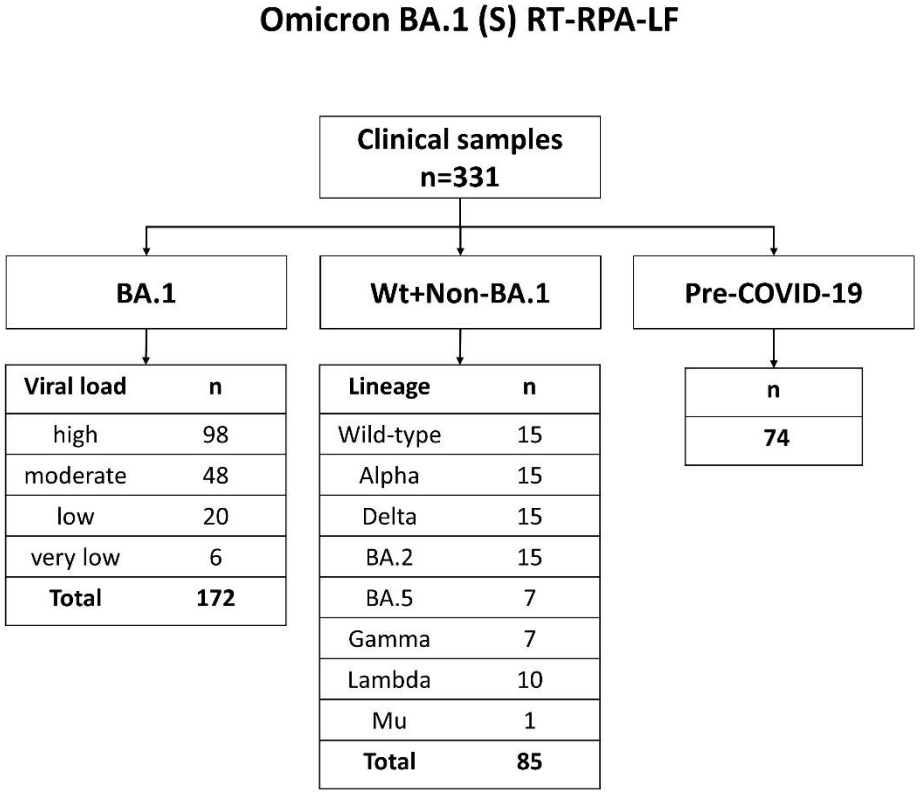

Figure 10. Flow chart of diagnostic evaluation for Omicron BA.1 (S) RT-RPA-LF.

BA1: Clinical samples classified as Omicron BA.1 using Sanger or NGS sequencing. Wt+Non-BA.1: Clinical samples classified as wild-type or VOC other than Omicron BA.1. Pre-COVID19: Clinical samples collected before the COVID-19. The viral loads were stratified as; Hight viral load: > 9777.3 copies/µL, moderate viral load: 503.5—9777.3 copies/µL, low viral load: 25.8—503.4 to copies/µL and very low viral load: < 25.8 copy/µL.

Wt: wild-type

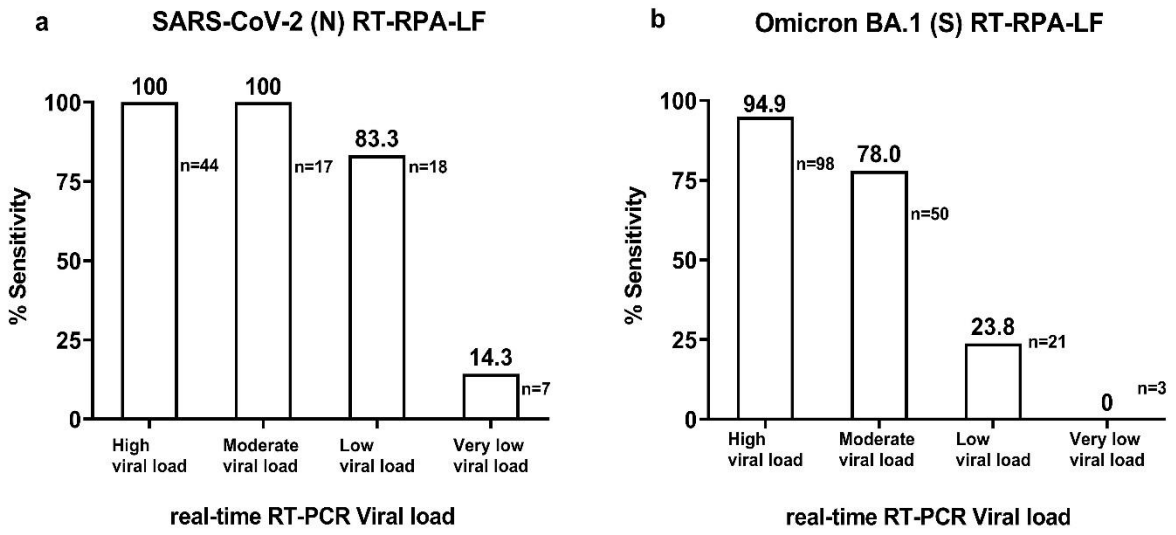

Figure 11. Sensitivity of SARS-CoV-2 (N) RT-RPA-LF and Omicron BA.1 (S) RT-RPA-LF tested in the clinical samples. **(a)** SARS-CoV-2 (N) RT-RPA-LF showed different sensitivities compared to real-time RT-PCR Cq values, **(b)** Omicron BA.1 (S) RT-RPA-LF showed different sensitivities compared to Cq values. Viral loads were classified as a high viral load: > 9,015.7 copies/µL, moderate viral load: 385.5–9,015.7 copies/µL, low viral load: 16.5–385.6 to copies/µL, and very low viral load: < 16.5 copies/µL.

9. Tables

Table 1. Consensus sequences for Omicron BA.1 and wild-type utilized for the generation of positive control (Omicron BA.1) and negative control SARS-CoV-2 (wild-type)

Name	Sequence (5'→3')	Length (nt)	Position	Reference
S_211del+214ins_wildtype	AAAAGTTGGATGGAAAGTGAGTTCAGAGTTTATTCTAGTGCGAATAATTGCACTTTTGAATATGTCTCTCAGCCTTTTCTTATGGACCTTGAAGGAAAACAGGGTAATTTCAAAAATCTTAGGGAATTTGTGTTTAAGAATATTGATGGTTATTTTAAAATATATTCTAAGCACACGCCTATTAATTTAGTGCGTGATCTCCCTCAGGGTTTTTCGGCTTTAGAACCATTGGTAGATTTGCCAATAGGTATTAACATCACTAGGTTTCAAACTTTACTTGCTTTACATAGAAGTTATTTGACTCCTGGTGATTCTTCTTCAGGTTGGACAGCTGGTGCTGCAGCTTATTATGTGGGTTATCTTCAACCTAGGACTTTTCTATTAAAATATAATGA	395	21984-22378	OL817641.1
S_211del+214ins_deleted	CAAAAACAACAAAAGTTGGATGGAAAGTGAGTTCAGAGTTTATTCTAGTGCGAATAATTGCACTTTTGAATATGTCTCTCAGCCTTTTCTTATGGACCTTGAAGGAAAACAGGGTAATTTCAAAAATCTTAGGGAATTTGTGTTTAAGAATATTGATGGTTATTTTAAAATATATTCTAAGCACACGCCTATTATAGTGCGTGAGCCAGAAGATCTCCCTCAGGGTTTTTCGGCTTTAGAACCATTGGTAGATTTGCCAATAGGTATTAACATCACTAGGTTTCAAACTTTACTTGCTTTACATAGAAGTTATTTGACTCCTGGTGATTCTTCTTCAGGTTGGACAGCTGGTGCTGCAGCTTATTATGTGGGTTATCTTCAACCTAGGACTTTT	394	21952-22345	OL822906.1

Table 2. Primers and probes designed in this study

RPA primers for the detection of SARS-CoV-2 and Omicron BA.1

Primer	The nucleotide sequence (5'→3')	GC (%)	Length (nt)	amplicon size (Bp)	Position	Genome reference
RPA_N_2F	GAACGTGGTTGACCTACACAGGTGCCATCAAAT	48.5	33	166	29203-29235	OP714083.1
RPA_N_2R-Bio	BIOTIN-GGTAAGGCTTGAGTTTCATCAGCCTTCTTCTTTT	41.2	34		29368-29335	OP714083.1
RPA_Probe_N1	FITC-ACAAAGATCCAAATTTCAAAGATCAAGTCA[THF]TTTGCTGAATAAGCA-C3	31.1	46	NA	29242-29287	OP714083.1
RPA_214ins_SET2_F	TCTTAGGGAATTTGTGTTTAAGAATATTGATGG	30.3	33	179	22072-22104	OP711808.1
RPA_214ins_SET2_R_Bio	Biotin- TATGTAAAGCAAGTAAAGTTTGAAACCTAGTG	31.3	32		22250-22219	OP711808.1
RPA_214INS_Probe_2	FITC-ACACGCCTATTATAGTGCGTGAGCCAGAA[THF]ATCTCCCTCAGGGTTT-C3	50.0	46	NA	22128-22173	OP711808.1

PCR primers adapted with theT7 promotor sequence utilized for the synthesis of RNA standards

PCR_T7_N_2F	*TAATACGACTCACTATAGG*GAACGTGGTTGACCTACACA	43.6	39	166	29203-29222	OP714083.1
PCR_T7__N_2R	GGTAAGGCTTGAGTTTCATCAG	45.5	22		29368-29347	OP714083.1
PCR_T7_214ins_SET2_F	*TAATACGACTCACTATAGG*GTAATTTCAAAAATCTTAG	28.1	38	185	22086-22103	ON062940.1
PCR_T7_214ins_SET2_R	TATGTAAAGCAAGTAAAGTT	25	20		22270-22251	ON062940.1

NA= Not applicable

Table 3. Clinical samples tested using SARS-CoV-2 (N) and Omicron BA.1 (S) RT-RPA-LF

RT-RPA-LF	Kawamura children clinic	Tohoku University Hospital[b]	Sendai City Institute of Public Health[c]	Virus Research Center, Sendai Medical Center[d]	Miyagi Prefectural Institute of Public Health and Environment[e]	Tohoku Kosai Hospital[f]	Universidad Peruana Cayetano Heredia[g]	Total
SARS-CoV-2 (N)	104	50	28	5	3	-	-	190
Omicron BA.1 (S)	74	56	-	-	128	40	33	331

In total, 454 samples were tested in this study. Of these, 190 were tested for SARS-CoV-2 (N) RT-RPA-LF, 331 were tested for Omicron BA.1 (S) RT-RPA-LF, and 67 were tested for both. Institutions a, b, d, e, and f used the QIAamp Viral RNA Mini Kit. The institution e used the MagMAX CORE Nucleic Acid Purification Kit and Maxwell RSC Total Nucleic Acid Purification Kit. The institution g used a Nucleic Acid Extraction-Purification kit (Sansure Biotech, China). Institutions b, c, d, e, and f used the SARS-CoV-2 PCR protocol (32), (33).

Table 4. Samples utilized for the cross-reactivity test

SARS-CoV-2 (N) RT-RPA-LF	Sample	Type	Cross-reactivity
	Human metapneumovirus	Clinical sample (cDNA)	No
	influenza A (H1N1)pdm09	Clinical sample (cDNA)	No
	Influenza C virus	Clinical sample (cDNA)	No
	Respiratory syncytial virus	Clinical sample (cDNA)	No
	Human parainfluenza virus type 1	Clinical sample (cDNA)	No
	Human parainfluenza virus type 2	Clinical sample (cDNA)	No
	Human parainfluenza virus type 3	Clinical sample (cDNA)	No
	Human parainfluenza virus type 4	Clinical sample (cDNA)	No
	Severe acute respiratory syndrome coronavirus	Bat SARS-like coronavirus isolate bat-SL-CoVZC45, genome standard (cDNA) (IDT, catalog 10006624)	No
	Middle east respiratory syndrome coronavirus	Middle East respiratory syndrome-related coronavirus isolate KNIH/002_05_2015, genome standard (cDNA) (IDT, catalog 10006623)	No
	Human coronavirus 229E	Human coronavirus 229E genome standard (ATCC-VR-740) (RNA)	No
	Human coronavirus OC43	Human coronavirus OC43 genome standard (ATCC-VR-1558) (RNA)	No
Omicron BA.1 (S) RT-RPA-LF	Alpha (B.1.1.7) VOC	Clinical sample (RNA)	No
	Delta (1.617.2) VOC	Clinical sample (RNA)	No
	Human coronavirus 229E	Human coronavirus 229E genome standard (ATCC-VR-740) (RNA)	No
	Human coronavirus OC43	Human coronavirus OC43 genome standard (ATCC-VR-1558) (RNA)	No
	Human coronavirus NL63	Clinical sample (RNA)	No
	Human coronavirus HKU1 (	Clinical sample (RNA)	No

cDNA: complementary DNA

Table 5

a. SARS-CoV-2 (N) RT-RPA-LF results by real-time RT-PCR using viral load categories.

	SARS-CoV-2 PCR positive (by viral load categories)				Pre-COVID-19	Total
RT-RPA	High (%)	Moderate (%)	Low (%)	Very low (%)		
Positive	44 (100.0)	17 (100.0)	15 (83.3)	1 (14.2)	0 (0.0)	77 (40.5)
Negative	0 (0.0)	0 (0.0)	3 (16.7)	6 (85.8)	104 (0.0)	113 (59.5)
Total	44 (100.0)	17 (100.0)	18 (100.0)	7 (100.0)	104 (100.0)	190 (100.0)

b. Omicron BA.1 (S) results of real-time RT-PCR using viral load categories.

	SARS-CoV-2 Omicron BA.1 (by viral load categories[a])				Non-BA.1 VOC	Pre - COVID-19	Total
RT-RPA-LF	High (%)	Moderate (%)	Low (%)	Very low (%)			
Positive	93 (94.9)	39 (78.0)	5(23.8)	0 (0.0)	3 (3.5)	3 (4.1)	143 (43.2)
Negative	5 (5.1)	11 (22.0)	16 (76.2)	3 (100.0)	82 (96.5)	71 (95.9)	188(56.8)
Total	98 (100.0)	50 (100.0)	21 (100)	3 (100.0)	85 (100)	74 (100.0)	331 (100.0)

VOC: Variant of concern. Viral loads were classified as high viral load: > 9,015.7 copies/µL, moderate viral load: 385.6–9,015.7 copies/µL, low viral load: 16.5–385.5 to copies/µL, and very low viral load: < 16.5 copies/µL.

Table 6.

PCR primers were used for the partial amplification and sequencing of the spike protein gene of the SARS-CoV-2 using the Sanger sequencing method

Primer Name	**Length (nt)**	**Sequence: 5'→3'**
SARS-CoV-2_S_38F	25	GTCAGTGTGTTAATCTTACAACCAG
SARS-CoV-2_S_1191R	25	TGCATAGACATTAGTAAAGCAGAGA
SARS-CoV-2-S-omi-1017F	20	TGAAGTTTTTAACGCCACCA
SARS-CoV-2_S_2249R	24	CTGCATTCAGTTGAATCACCACAA
SARS-CoV-2-S-omi-663R	20	CGAAAAACCCTGAGGGAGAT
SARS-CoV-2-S-omi-486F	21	TGCGAATAATTGCACTTTTGA
SARS-CoV-2_S_1583R	21	TTAGGTCCACAAACAGTTGCT
SARS-CoV-2-S-omi-1363F	26	TTGTTTAGGAAGTCTAATCTCAAACC

nt = nucleotides

Table 7.

Sensitivity of some rapid assay for SARS-CoV-2 on clinical samples under different viral load values

Test	Method	Sensitivity (%) by viral load				Target
		High	Moderate	Low	Very low	
SARS-CoV-2 (N) RT-RPA-LF*	RT-RPA	44/44 (100)	17/17 (100)	15/18 (83)	1/7 (14)	SARS-CoV-2 (N)
Omicron BA.1 (S) RT-RPA-LF*	RT-RPA	93/98 (95)	39/50 (78)	5/21 (24)	0/3 (0)	Omicron BA.1 (S)
Colorimetric RT-LAMP [64]	RT-LAMP	51/51 (100)	28/30 (93)	4/20 (20)	0/16 (0)	SARS-CoV-2
BD Veritor [52]	LFAs	13/13 (100)	10/14 (71)	0/8 (0)	1/13 (8)	SARS-CoV-2
Sofia 2 SARS Ag [52]	LFAs	13/13 (100)	12/14 (86)	1/8 (13)	1/13 (8)	SARS-CoV-2
BinaxNOW [52]	LFAs	13/13 (100)	11/14 (79)	1/8 (13)	1/13 (8)	SARS-CoV-2
Standard Q COVID-19 Ag [51]	LFA	4/4 (100)	18/24 (75)	5/37 (14)	0/11 (0)	SARS-CoV-2
Espline SARS-CoV-2 [51]	LFA	4/4 (100)	20/24 (83)	4/37 (11)	0/11 (0)	SARS-CoV-2
QuickNavi COVID19 Ag [51]	LFA	4/4 (100)	10/24 (42)	2/37 (5)	0/11 (0)	SARS-CoV-2

RT-LAMP: Reverse transcription loop-mediated amplification. LFA: Lateral flow antigen detection assays. N: Nucleocapsid protein gene, S: Spike protein gene.

* Test developed in this study.

Table 8. List of sequences used for the clinical evaluation of the Omicron (S) BA.1 RT-RPA-LF

Number	Lineage	Country	Accession number
1.	Omicron BA.1	Japan	EPI_ISL_13208893
2.	Omicron BA.1	Japan	EPI_ISL_13209110
3.	Omicron BA.1	Japan	EPI_ISL_14110653
4.	Omicron BA.5	Japan	EPI_ISL_14125573
5.	Omicron BA.5	Japan	EPI_ISL_14125574
6.	Omicron BA.5	Japan	EPI_ISL_14125575
7.	Omicron BA.5	Japan	EPI_ISL_14139800
8.	Omicron BA.5	Japan	EPI_ISL_14139805
9.	Omicron BA.5	Japan	EPI_ISL_14139806
10.	Wild-type	Japan	EPI_ISL_17263993
11.	Wild-type	Japan	EPI_ISL_17263994
12.	Wild-type	Japan	EPI_ISL_17263995
13.	Wild-type	Japan	EPI_ISL_17263996
14.	Wild-type	Japan	EPI_ISL_17263997
15.	Wild-type	Japan	EPI_ISL_17263998
16.	Wild-type	Japan	EPI_ISL_17263999
17.	Wild-type	Japan	EPI_ISL_17264000
18.	Wild-type	Japan	EPI_ISL_17264001
19.	Wild-type	Japan	EPI_ISL_17264002
20.	Wild-type	Japan	EPI_ISL_17264003
21.	Wild-type	Japan	EPI_ISL_17264004
22.	Wild-type	Japan	EPI_ISL_17264005
23.	Wild-type	Japan	EPI_ISL_17264006
24.	Wild-type	Japan	EPI_ISL_17264007
25.	Alpha	Japan	EPI_ISL_17264009
26.	Alpha	Japan	EPI_ISL_17264010
27.	Alpha	Japan	EPI_ISL_17264011
28.	Alpha	Japan	EPI_ISL_17264012
29.	Alpha	Japan	EPI_ISL_17264013
30.	Alpha	Japan	EPI_ISL_17264014
31.	Alpha	Japan	EPI_ISL_17264015
32.	Alpha	Japan	EPI_ISL_17264016
33.	Alpha	Japan	EPI_ISL_17264017
34.	Alpha	Japan	EPI_ISL_17264018
35.	Alpha	Japan	EPI_ISL_17264019
36.	Alpha	Japan	EPI_ISL_17267731
37.	Alpha	Japan	EPI_ISL_17264020
38.	Alpha	Japan	EPI_ISL_17264021
39.	Alpha	Japan	EPI_ISL_17264022
40.	Omicron BA.1	Japan	EPI_ISL_17264023

41.	Omicron BA.1	Japan	EPI_ISL_17264024
42.	Omicron BA.1	Japan	EPI_ISL_17264025
43.	Omicron BA.1	Japan	EPI_ISL_17264026
44.	Omicron BA.1	Japan	EPI_ISL_17264027
45.	Omicron BA.1	Japan	EPI_ISL_17264028
46.	Omicron BA.1	Japan	EPI_ISL_17264029
47.	Omicron BA.1	Japan	EPI_ISL_17264030
48.	Omicron BA.1	Japan	EPI_ISL_17264031
49.	Omicron BA.1	Japan	EPI_ISL_17264032
50.	Omicron BA.1	Japan	EPI_ISL_17264033
51.	Omicron BA.1	Japan	EPI_ISL_17264034
52.	Omicron BA.1	Japan	EPI_ISL_17264035
53.	Omicron BA.1	Japan	EPI_ISL_17264036
54.	Omicron BA.1	Japan	EPI_ISL_17264037
55.	Omicron BA.1	Japan	EPI_ISL_17267732
56.	Omicron BA.1	Japan	EPI_ISL_17264038
57.	Omicron BA.1	Japan	EPI_ISL_17264039
58.	Omicron BA.1	Japan	EPI_ISL_17264040
59.	Omicron BA.1	Japan	EPI_ISL_17264041
60.	Omicron BA.1	Japan	EPI_ISL_17264042
61.	Omicron BA.1	Japan	EPI_ISL_17264043
62.	Omicron BA.1	Japan	EPI_ISL_17264044
63.	Omicron BA.1	Japan	EPI_ISL_17264045
64.	Omicron BA.1	Japan	EPI_ISL_17264046
65.	Omicron BA.1	Japan	EPI_ISL_17264047
66.	Omicron BA.1	Japan	EPI_ISL_17264048
67.	Omicron BA.1	Japan	EPI_ISL_17264049
68.	Omicron BA.1	Japan	EPI_ISL_17264050
69.	Omicron BA.1	Japan	EPI_ISL_17264051
70.	Omicron BA.1	Japan	EPI_ISL_17264052
71.	Omicron BA.1	Japan	EPI_ISL_17264053
72.	Omicron BA.1	Japan	EPI_ISL_17264054
73.	Omicron BA.1	Japan	EPI_ISL_17264055
74.	Omicron BA.1	Japan	EPI_ISL_17264056
75.	Omicron BA.1	Japan	EPI_ISL_17264057
76.	Omicron BA.1	Japan	EPI_ISL_17264058
77.	Omicron BA.1	Japan	EPI_ISL_17264059
78.	Omicron BA.1	Japan	EPI_ISL_17264060
79.	Omicron BA.1	Japan	EPI_ISL_17264061
80.	Omicron BA.1	Japan	EPI_ISL_17264062
81.	Omicron BA.1	Japan	EPI_ISL_17264063
82.	Omicron BA.1	Japan	EPI_ISL_17264064
83.	Omicron BA.1	Japan	EPI_ISL_17264065
84.	Omicron BA.1	Japan	EPI_ISL_17264066

85.	Omicron BA.1	Japan	EPI_ISL_17264067
86.	Omicron BA.1	Japan	EPI_ISL_17264068
87.	Omicron BA.1	Japan	EPI_ISL_17264069
88.	Omicron BA.1	Japan	EPI_ISL_17264070
89.	Omicron BA.1	Japan	EPI_ISL_17264071
90.	Omicron BA.1	Japan	EPI_ISL_17264072
91.	Omicron BA.1	Japan	EPI_ISL_17264073
92.	Omicron BA.1	Japan	EPI_ISL_17264074
93.	Omicron BA.1	Japan	EPI_ISL_17264075
94.	Omicron BA.1	Japan	EPI_ISL_17264076
95.	Omicron BA.1	Japan	EPI_ISL_17264077
96.	Omicron BA.1	Japan	EPI_ISL_17264078
97.	Omicron BA.1	Japan	EPI_ISL_17264079
98.	Omicron BA.1	Japan	EPI_ISL_17264080
99.	Omicron BA.1	Japan	EPI_ISL_17264081
100.	Omicron BA.1	Japan	EPI_ISL_17264082
101.	Omicron BA.1	Japan	EPI_ISL_17264083
102.	Omicron BA.1	Japan	EPI_ISL_17264084
103.	Omicron BA.1	Japan	EPI_ISL_17264085
104.	Omicron BA.1	Japan	EPI_ISL_17264086
105.	Omicron BA.1	Japan	EPI_ISL_17264087
106.	Omicron BA.1	Japan	EPI_ISL_17264088
107.	Omicron BA.1	Japan	EPI_ISL_17264089
108.	Omicron BA.1	Japan	EPI_ISL_17264091
109.	Omicron BA.1	Japan	EPI_ISL_17264092
110.	Omicron BA.1	Japan	EPI_ISL_17264093
111.	Omicron BA.1	Japan	EPI_ISL_17264094
112.	Omicron BA.1	Japan	EPI_ISL_17264095
113.	Omicron BA.1	Japan	EPI_ISL_17264096
114.	Omicron BA.1	Japan	EPI_ISL_17264097
115.	Omicron BA.1	Japan	EPI_ISL_17264098
116.	Omicron BA.1	Japan	EPI_ISL_17264099
117.	Omicron BA.1	Japan	EPI_ISL_17264100
118.	Omicron BA.1	Japan	EPI_ISL_17264101
119.	Omicron BA.1	Japan	EPI_ISL_17264102
120.	Omicron BA.1	Japan	EPI_ISL_17264103
121.	Omicron BA.1	Japan	EPI_ISL_17264104
122.	Omicron BA.1	Japan	EPI_ISL_17264105
123.	Omicron BA.1	Japan	EPI_ISL_17264106
124.	Omicron BA.1	Japan	EPI_ISL_17264107
125.	Omicron BA.1	Japan	EPI_ISL_17264108
126.	Omicron BA.1	Japan	EPI_ISL_17264109
127.	Omicron BA.1	Japan	EPI_ISL_17264110
128.	Omicron BA.1	Japan	EPI_ISL_17264111

129.	Omicron BA.1	Japan	EPI_ISL_17264112
130.	Omicron BA.1	Japan	EPI_ISL_17264113
131.	Omicron BA.1	Japan	EPI_ISL_17264114
132.	Omicron BA.1	Japan	EPI_ISL_17264115
133.	Omicron BA.1	Japan	EPI_ISL_17264116
134.	Omicron BA.1	Japan	EPI_ISL_17264117
135.	Omicron BA.1	Japan	EPI_ISL_17264118
136.	Omicron BA.1	Japan	EPI_ISL_17264119
137.	Omicron BA.1	Japan	EPI_ISL_17264120
138.	Omicron BA.1	Japan	EPI_ISL_17264121
139.	Omicron BA.1	Japan	EPI_ISL_17264122
140.	Omicron BA.1	Japan	EPI_ISL_17264123
141.	Omicron BA.1	Japan	EPI_ISL_17264124
142.	Omicron BA.1	Japan	EPI_ISL_17264125
143.	Omicron BA.1	Japan	EPI_ISL_17264126
144.	Omicron BA.1	Japan	EPI_ISL_17264127
145.	Omicron BA.1	Japan	EPI_ISL_17264128
146.	Omicron BA.1	Japan	EPI_ISL_17264129
147.	Omicron BA.1	Japan	EPI_ISL_17264130
148.	Omicron BA.1	Japan	EPI_ISL_17264131
149.	Omicron BA.1	Japan	EPI_ISL_17264132
150.	Omicron BA.1	Japan	EPI_ISL_17264133
151.	Omicron BA.1	Japan	EPI_ISL_17264134
152.	Omicron BA.1	Japan	EPI_ISL_17264135
153.	Omicron BA.1	Japan	EPI_ISL_17264136
154.	Omicron BA.1	Japan	EPI_ISL_17264137
155.	Omicron BA.1	Japan	EPI_ISL_17264138
156.	Omicron BA.1	Japan	EPI_ISL_17264139
157.	Omicron BA.1	Japan	EPI_ISL_17264140
158.	Omicron BA.1	Japan	EPI_ISL_17264141
159.	Omicron BA.1	Japan	EPI_ISL_17264142
160.	Omicron BA.1	Japan	EPI_ISL_17264143
161.	Omicron BA.2	Japan	EPI_ISL_17264144
162.	Omicron BA.1	Japan	EPI_ISL_17264145
163.	Omicron BA.2	Japan	EPI_ISL_17264146
164.	Omicron BA.1	Japan	EPI_ISL_17264147
165.	Omicron BA.1	Japan	EPI_ISL_17264148
166.	Omicron BA.1	Japan	EPI_ISL_17264149
167.	Omicron BA.1	Japan	EPI_ISL_17264150
168.	Omicron BA.1	Japan	EPI_ISL_17264151
169.	Omicron BA.1	Japan	EPI_ISL_17264152
170.	Omicron BA.1	Japan	EPI_ISL_17264153
171.	Omicron BA.1	Japan	EPI_ISL_17264154
172.	Omicron BA.1	Japan	EPI_ISL_17264155

173.	Omicron BA.1	Japan	EPI_ISL_17264156
174.	Omicron BA.1	Japan	EPI_ISL_17264157
175.	Omicron BA.1	Japan	EPI_ISL_17264158
176.	Omicron BA.1	Japan	EPI_ISL_17264159
177.	Omicron BA.1	Japan	EPI_ISL_17264160
178.	Omicron BA.1	Japan	EPI_ISL_17264161
179.	Omicron BA.1	Japan	EPI_ISL_17264162
180.	Omicron BA.1	Japan	EPI_ISL_17264163
181.	Omicron BA.1	Japan	EPI_ISL_17264164
182.	Omicron BA.1	Japan	EPI_ISL_17264165
183.	Omicron BA.1	Japan	EPI_ISL_17264166
184.	Omicron BA.2	Japan	EPI_ISL_17264167
185.	Omicron BA.2	Japan	EPI_ISL_17264168
186.	Omicron BA.1	Japan	EPI_ISL_17264169
187.	Omicron BA.2	Japan	EPI_ISL_17264170
188.	Omicron BA.1	Japan	EPI_ISL_17264171
189.	Omicron BA.1	Japan	EPI_ISL_17264172
190.	Omicron BA.1	Japan	EPI_ISL_17264173
191.	Omicron BA.1	Japan	EPI_ISL_17264174
192.	Omicron BA.1	Japan	EPI_ISL_17264175
193.	Omicron BA.1	Japan	EPI_ISL_17264176
194.	Omicron BA.1	Japan	EPI_ISL_17264177
195.	Omicron BA.2	Japan	EPI_ISL_17264179
196.	Omicron BA.1	Japan	EPI_ISL_17264180
197.	Omicron BA.1	Japan	EPI_ISL_17264181
198.	Omicron BA.1	Japan	EPI_ISL_17264182
199.	Omicron BA.1	Japan	EPI_ISL_17264183
200.	Omicron BA.1	Japan	EPI_ISL_17264184
201.	Omicron BA.1	Japan	EPI_ISL_17264185
202.	Omicron BA.1	Japan	EPI_ISL_17264186
203.	Omicron BA.1	Japan	EPI_ISL_17264187
204.	Omicron BA.2	Japan	EPI_ISL_17264188
205.	Omicron BA.1	Japan	EPI_ISL_17264189
206.	Omicron BA.1	Japan	EPI_ISL_17264190
207.	Omicron BA.1	Japan	EPI_ISL_17264191
208.	Omicron BA.2	Japan	EPI_ISL_17264192
209.	Omicron BA.2	Japan	EPI_ISL_17264193
210.	Omicron BA.1	Japan	EPI_ISL_17264194
211.	Omicron BA.2	Japan	EPI_ISL_17264195
212.	Omicron BA.1	Japan	EPI_ISL_17264196
213.	Omicron BA.1	Japan	EPI_ISL_17264197
214.	Omicron BA.2	Japan	EPI_ISL_17264198
215.	Omicron BA.1	Japan	EPI_ISL_17264199
216.	Omicron BA.2	Japan	EPI_ISL_17264200

217.	Omicron BA.2	Japan	EPI_ISL_17264201
218.	Omicron BA.1	Japan	EPI_ISL_17264202
219.	Omicron BA.1	Japan	EPI_ISL_17264203
220.	Omicron BA.2	Japan	EPI_ISL_17264204
221.	Omicron BA.1	Japan	EPI_ISL_17264205
222.	Omicron BA.2	Japan	EPI_ISL_17264206
223.	Omicron BA.1	Japan	EPI_ISL_17264207
224.	Omicron BA.5	Japan	EPI_ISL_17264208
225.	Gamma	Peru	EPI_ISL_5147044
226.	Gamma	Peru	EPI_ISL_5147024
227.	Gamma	Peru	EPI_ISL_5147060
228.	Gamma	Peru	EPI_ISL_5147025
229.	Gamma	Peru	EPI_ISL_7961373
230.	Gamma	Peru	EPI_ISL_7961347
231.	Gamma	Peru	EPI_ISL_7961375
232.	Lambda	Peru	EPI_ISL_5147099
233.	Lambda	Peru	EPI_ISL_5147665
234.	Lambda	Peru	EPI_ISL_5147100
235.	Lambda	Peru	EPI_ISL_5147101
236.	Lambda	Peru	EPI_ISL_5146989
237.	Lambda	Peru	EPI_ISL_5147146
238.	Lambda	Peru	EPI_ISL_5147103
239.	Lambda	Peru	EPI_ISL_5147104
240.	Lambda	Peru	EPI_ISL_5146994
241.	Lambda	Peru	EPI_ISL_5147152
242.	Mu	Peru	EPI_ISL_7961381
243.	Delta	Peru	EPI_ISL_7961304
244.	Delta	Peru	EPI_ISL_7961473
245.	Delta	Peru	EPI_ISL_7961310
246.	Delta	Peru	EPI_ISL_7961291
247.	Delta	Peru	EPI_ISL_7961474
248.	Delta	Peru	EPI_ISL_7961475
249.	Delta	Peru	EPI_ISL_7961333
250.	Delta	Peru	EPI_ISL_7961247
251.	Delta	Peru	EPI_ISL_7961339
252.	Delta	Peru	EPI_ISL_7961268
253.	Delta	Peru	EPI_ISL_7961476
254.	Delta	Peru	EPI_ISL_9637468
255.	Delta	Peru	EPI_ISL_9637469
256.	Delta	Peru	EPI_ISL_9637471
257.	Delta	Peru	EPI_ISL_9637473

10. References

(1) Perlman, S.; Masters, P. Coronaviridae: The Viruses and Their Replication. In *Fields Virology, Emerging Viruses*; Howley, P., Knipe, D., Eds.; 2021; Vol. 1, pp 410–440.

(2) Wang, M. Y.; Zhao, R.; Gao, L. J.; Gao, X. F.; Wang, D. P.; Cao, J. M. SARS-CoV-2: Structure, Biology, and Structure-Based Therapeutics Development. *Frontiers in Cellular and Infection Microbiology*. Frontiers Media S.A. November 25, 2020. https://doi.org/10.3389/fcimb.2020.587269.

(3) Goldstein, S.; Hogus, B.; Leibowitz, J.; Weiss, S. *Fields Virology, RNA Viruses*, Seventh.; Howley, P., Knipe, D., Eds.; 2023; Vol. 3.

(4) Tang, Y.-W.; Schmitz, J. E.; Persing, D. H.; Stratton, C. W. *Laboratory Diagnosis of COVID-19: Current Issues and Challenges*; 2020. https://journals.asm.org/journal/jcm.

(5) *CDC 2019-Novel Coronavirus (2019-NCoV) Real-Time RT-PCR Diagnostic Panel For Emergency Use Only Instructions for Use*. https://www.fda.gov/media/134922/download (accessed 2023-04-10).

(6) Sheikh, A.; Al-Taher, A.; Al-Nazawi, M.; Al-Mubarak, A. I.; Kandeel, M. Analysis of Preferred Codon Usage in the Coronavirus N Genes and Their Implications for Genome Evolution and Vaccine Design. *J Virol Methods* **2020**, *277*. https://doi.org/10.1016/j.jviromet.2019.113806.

(7) Hiscox, J. A.; Cavanagh, D.; Britton, P. *Quantification of Individual Subgenomic MRNA Species during Replication of the Coronavirus Transmissible Gastroenteritis Virus*; 1995.

(8) Vogels, C. B. F.; Brito, A. F.; Wyllie, A. L.; Fauver, J. R.; Ott, I. M.; Kalinich, C. C.; Petrone, M. E.; Casanovas-Massana, A.; Catherine Muenker, M.; Moore, A. J.; Klein, J.; Lu, P.; Lu-Culligan, A.; Jiang, X.; Kim, D. J.; Kudo, E.; Mao, T.; Moriyama, M.; Oh, J. E.; Park, A.; Silva, J.; Song, E.; Takahashi, T.; Taura, M.; Tokuyama, M.; Venkataraman, A.; Weizman, O. El; Wong, P.; Yang, Y.; Cheemarla, N. R.; White, E. B.; Lapidus, S.; Earnest, R.; Geng, B.; Vijayakumar, P.; Odio, C.; Fournier, J.; Bermejo, S.; Farhadian, S.; Dela Cruz, C. S.; Iwasaki, A.; Ko, A. I.; Landry, M. L.; Foxman, E. F.; Grubaugh, N. D. Analytical Sensitivity and Efficiency Comparisons of SARS-CoV-2 RT–QPCR Primer–Probe Sets. *Nat Microbiol* **2020**, *5* (10), 1299–1305. https://doi.org/10.1038/s41564-020-0761-6.

(9) Abbasian, M. H.; Mahmanzar, M.; Rahimian, K.; Mahdavi, B.; Tokhanbigli, S.; Moradi, B.; Sisakht, M. M.; Deng, Y. Global Landscape of SARS-CoV-2 Mutations and Conserved Regions. *J Transl Med* **2023**, *21* (1). https://doi.org/10.1186/s12967-023-03996-w.

(10) Walls, A. C.; Park, Y. J.; Tortorici, M. A.; Wall, A.; McGuire, A. T.; Veesler, D. Structure, Function, and Antigenicity of the SARS-CoV-2 Spike Glycoprotein. *Cell* **2020**, *181* (2), 281-292.e6. https://doi.org/10.1016/j.cell.2020.02.058.

(11) Korber, B.; Fischer, W. M.; Gnanakaran, S.; Yoon, H.; Theiler, J.; Abfalterer, W.; Hengartner, N.; Giorgi, E. E.; Bhattacharya, T.; Foley, B.; Hastie, K. M.; Parker, M. D.; Partridge, D. G.; Evans, C. M.; Freeman, T. M.; de Silva, T. I.; Angyal, A.; Brown, R. L.; Carrilero, L.; Green, L. R.; Groves, D. C.; Johnson, K. J.; Keeley, A. J.; Lindsey, B. B.; Parsons, P. J.; Raza, M.; Rowland-Jones, S.; Smith, N.; Tucker, R. M.; Wang, D.; Wyles, M. D.; McDanal, C.; Perez, L. G.; Tang, H.; Moon-Walker, A.; Whelan, S. P.; LaBranche, C. C.; Saphire, E. O.; Montefiori, D. C. Tracking Changes in SARS-CoV-2

Spike: Evidence That D614G Increases Infectivity of the COVID-19 Virus. *Cell* **2020**, *182* (4), 812-827.e19. https://doi.org/10.1016/j.cell.2020.06.043.

(12) Volz, E.; Hill, V.; McCrone, J. T.; Price, A.; Jorgensen, D.; O'Toole, Á.; Southgate, J.; Johnson, R.; Jackson, B.; Nascimento, F. F.; Rey, S. M.; Nicholls, S. M.; Colquhoun, R. M.; da Silva Filipe, A.; Shepherd, J.; Pascall, D. J.; Shah, R.; Jesudason, N.; Li, K.; Jarrett, R.; Pacchiarini, N.; Bull, M.; Geidelberg, L.; Siveroni, I.; Koshy, C.; Wise, E.; Cortes, N.; Lynch, J.; Kidd, S.; Mori, M.; Fairley, D. J.; Curran, T.; McKenna, J. P.; Adams, H.; Fraser, C.; Golubchik, T.; Bonsall, D.; Moore, C.; Caddy, S. L.; Khokhar, F. A.; Wantoch, M.; Reynolds, N.; Warne, B.; Maksimovic, J.; Spellman, K.; McCluggage, K.; John, M.; Beer, R.; Afifi, S.; Morgan, S.; Marchbank, A.; Kitchen, C.; Gulliver, H.; Merrick, I.; Guest, M.; Munn, R.; Workman, T.; Connor, T. R.; Fuller, W.; Bresner, C.; Snell, L. B.; Charalampous, T.; Nebbia, G.; Batra, R.; Edgeworth, J.; Robson, S. C.; Beckett, A.; Loveson, K. F.; Aanensen, D. M.; Underwood, A. P.; Yeats, C. A.; Abudahab, K.; Taylor, B. E. W.; Menegazzo, M.; Clark, G.; Smith, W.; Khakh, M.; Fleming, V. M.; Lister, M. M.; Howson-Wells, H. C.; Berry, L.; Boswell, T.; Joseph, A.; Willingham, I.; Bird, P.; Helmer, T.; Fallon, K.; Holmes, C.; Tang, J.; Raviprakash, V.; Campbell, S.; Sheriff, N.; Loose, M. W.; Holmes, N.; Moore, C.; Carlile, M.; Wright, V.; Sang, F.; Debebe, J.; Coll, F.; Signell, A. W.; Betancor, G.; Wilson, H. D.; Feltwell, T.; Houldcroft, C. J.; Eldirdiri, S.; Kenyon, A.; Davis, T.; Pybus, O.; du Plessis, L.; Zarebski, A.; Raghwani, J.; Kraemer, M.; Francois, S.; Attwood, S.; Vasylyeva, T.; Torok, M. E.; Hamilton, W. L.; Goodfellow, I. G.; Hall, G.; Jahun, A. S.; Chaudhry, Y.; Hosmillo, M.; Pinckert, M. L.; Georgana, I.; Yakovleva, A.; Meredith, L. W.; Moses, S.; Lowe, H.; Ryan, F.; Fisher, C. L.; Awan, A. R.; Boyes, J.; Breuer, J.; Harris, K. A.; Brown, J. R.; Shah, D.; Atkinson, L.; Lee, J. C. D.; Alcolea-Medina, A.; Moore, N.; Cortes, N.; Williams, R.; Chapman, M. R.; Levett, L. J.; Heaney, J.; Smith, D. L.; Bashton, M.; Young, G. R.; Allan, J.; Loh, J.; Randell, P. A.; Cox, A.; Madona, P.; Holmes, A.; Bolt, F.; Price, J.; Mookerjee, S.; Rowan, A.; Taylor, G. P.; Ragonnet-Cronin, M.; Johnson, R.; Boyd, O.; Volz, E. M.; Brunker, K.; Smollett, K. L.; Loman, N. J.; Quick, J.; McMurray, C.; Stockton, J.; Nicholls, S.; Rowe, W.; Poplawski, R.; Martinez-Nunez, R. T.; Mason, J.; Robinson, T. I.; O'Toole, E.; Watts, J.; Breen, C.; Cowell, A.; Ludden, C.; Sluga, G.; Machin, N. W.; Ahmad, S. S. Y.; George, R. P.; Halstead, F.; Sivaprakasam, V.; Thomson, E. C.; Shepherd, J. G.; Asamaphan, P.; Niebel, M. O.; Li, K. K.; Shah, R. N.; Jesudason, N. G.; Parr, Y. A.; Tong, L.; Broos, A.; Mair, D.; Nichols, J.; Carmichael, S. N.; Nomikou, K.; Aranday-Cortes, E.; Johnson, N.; Starinskij, I.; Robertson, D. L.; Orton, R. J.; Hughes, J.; Vattipally, S.; Singer, J. B.; Hale, A. D.; Macfarlane-Smith, L. R.; Harper, K. L.; Taha, Y.; Payne, B. A. I.; Burton-Fanning, S.; Waugh, S.; Collins, J.; Eltringham, G.; Templeton, K. E.; McHugh, M. P.; Dewar, R.; Wastenge, E.; Dervisevic, S.; Stanley, R.; Prakash, R.; Stuart, C.; Elumogo, N.; Sethi, D. K.; Meader, E. J.; Coupland, L. J.; Potter, W.; Graham, C.; Barton, E.; Padgett, D.; Scott, G.; Swindells, E.; Greenaway, J.; Nelson, A.; Yew, W. C.; Resende Silva, P. C.; Andersson, M.; Shaw, R.; Peto, T.; Justice, A.; Eyre, D.; Crooke, D.; Hoosdally, S.; Sloan, T. J.; Duckworth, N.; Walsh, S.; Chauhan, A. J.; Glaysher, S.; Bicknell, K.; Wyllie, S.; Butcher, E.; Elliott, S.; Lloyd, A.; Impey, R.; Levene, N.; Monaghan, L.; Bradley, D. T.; Allara, E.; Pearson, C.; Muir, P.; Vipond, I. B.; Hopes, R.; Pymont, H. M.; Hutchings, S.; Curran, M. D.; Parmar, S.; Lackenby, A.; Mbisa, T.; Platt, S.; Miah, S.; Bibby, D.; Manso, C.; Hubb, J.; Chand, M.; Dabrera, G.; Ramsay, M.; Bradshaw, D.; Thornton, A.; Myers, R.; Schaefer, U.; Groves, N.; Gallagher, E.; Lee, D.; Williams, D.; Ellaby, N.; Harrison, I.; Hartman, H.; Manesis, N.; Patel, V.; Bishop, C.; Chalker, V.; Osman, H.; Bosworth, A.; Robinson, E.; Holden, M. T. G.; Shaaban, S.; Birchley, A.; Adams, A.; Davies, A.; Gaskin, A.; Plimmer, A.; Gatica-Wilcox, B.; McKerr, C.; Moore, C.; Williams, C.; Heyburn, D.; De Lacy, E.; Hilvers, E.; Downing, F.;

Shankar, G.; Jones, H.; Asad, H.; Coombes, J.; Watkins, J.; Evans, J. M.; Fina, L.; Gifford, L.; Gilbert, L.; Graham, L.; Perry, M.; Morgan, M.; Cronin, M.; Craine, N.; Jones, R.; Howe, R.; Corden, S.; Rey, S.; Kumziene-Summerhayes, S.; Taylor, S.; Cottrell, S.; Jones, S.; Edwards, S.; O'Grady, J.; Page, A. J.; Wain, J.; Webber, M. A.; Mather, A. E.; Baker, D. J.; Rudder, S.; Yasir, M.; Thomson, N. M.; Aydin, A.; Tedim, A. P.; Kay, G. L.; Trotter, A. J.; Gilroy, R. A. J.; Alikhan, N. F.; de Oliveira Martins, L.; Le-Viet, T.; Meadows, L.; Kolyva, A.; Diaz, M.; Bell, A.; Gutierrez, A. V.; Charles, I. G.; Adriaenssens, E. M.; Kingsley, R. A.; Casey, A.; Simpson, D. A.; Molnar, Z.; Thompson, T.; Acheson, E.; Masoli, J. A. H.; Knight, B. A.; Hattersley, A.; Ellard, S.; Auckland, C.; Mahungu, T. W.; Irish-Tavares, D.; Haque, T.; Bourgeois, Y.; Scarlett, G. P.; Partridge, D. G.; Raza, M.; Evans, C.; Johnson, K.; Liggett, S.; Baker, P.; Essex, S.; Lyons, R. A.; Caller, L. G.; Castellano, S.; Williams, R. J.; Kristiansen, M.; Roy, S.; Williams, C. A.; Dyal, P. L.; Tutill, H. J.; Panchbhaya, Y. N.; Forrest, L. M.; Niola, P.; Findlay, J.; Brooks, T. T.; Gavriil, A.; Mestek-Boukhibar, L.; Weeks, S.; Pandey, S.; Berry, L.; Jones, K.; Richter, A.; Beggs, A.; Smith, C. P.; Bucca, G.; Hesketh, A. R.; Harrison, E. M.; Peacock, S. J.; Palmer, S.; Churcher, C. M.; Bellis, K. L.; Girgis, S. T.; Naydenova, P.; Blane, B.; Sridhar, S.; Ruis, C.; Forrest, S.; Cormie, C.; Gill, H. K.; Dias, J.; Higginson, E. E.; Maes, M.; Young, J.; Kermack, L. M.; Hadjirin, N. F.; Aggarwal, D.; Griffith, L.; Swingler, T.; Davidson, R. K.; Rambaut, A.; Williams, T.; Balcazar, C. E.; Gallagher, M. D.; O'Toole, Á.; Rooke, S.; Colquhoun, R.; Ashworth, J.; McCrone, J. T.; Scher, E.; Yu, X.; Williamson, K. A.; Stanton, T. D.; Michell, S. L.; Bewshea, C. M.; Temperton, B.; Michelsen, M. L.; Warwick-Dugdale, J.; Manley, R.; Farbos, A.; Harrison, J. W.; Sambles, C. M.; Studholme, D. J.; Jeffries, A. R.; Darby, A. C.; Hiscox, J. A.; Paterson, S.; Iturriza-Gomara, M.; Jackson, K. A.; Lucaci, A. O.; Vamos, E. E.; Hughes, M.; Rainbow, L.; Eccles, R.; Nelson, C.; Whitehead, M.; Turtle, L.; Haldenby, S. T.; Gregory, R.; Gemmell, M.; Kwiatkowski, D.; de Silva, T. I.; Smith, N.; Angyal, A.; Lindsey, B. B.; Groves, D. C.; Green, L. R.; Wang, D.; Freeman, T. M.; Parker, M. D.; Keeley, A. J.; Parsons, P. J.; Tucker, R. M.; Brown, R.; Wyles, M.; Constantinidou, C.; Unnikrishnan, M.; Ott, S.; Cheng, J. K. J.; Bridgewater, H. E.; Frost, L. R.; Taylor-Joyce, G.; Stark, R.; Baxter, L.; Alam, M. T.; Brown, P. E.; McClure, P. C.; Chappell, J. G.; Tsoleridis, T.; Ball, J.; Gramatopoulos, D.; Buck, D.; Todd, J. A.; Green, A.; Trebes, A.; MacIntyre-Cockett, G.; de Cesare, M.; Langford, C.; Alderton, A.; Amato, R.; Goncalves, S.; Jackson, D. K.; Johnston, I.; Sillitoe, J.; Palmer, S.; Lawniczak, M.; Berriman, M.; Danesh, J.; Livett, R.; Shirley, L.; Farr, B.; Quail, M.; Thurston, S.; Park, N.; Betteridge, E.; Weldon, D.; Goodwin, S.; Nelson, R.; Beaver, C.; Letchford, L.; Jackson, D. A.; Foulser, L.; McMinn, L.; Prestwood, L.; Kay, S.; Kane, L.; Dorman, M. J.; Martincorena, I.; Puethe, C.; Keatley, J. P.; Tonkin-Hill, G.; Smith, C.; Jamrozy, D.; Beale, M. A.; Patel, M.; Ariani, C.; Spencer-Chapman, M.; Drury, E.; Lo, S.; Rajatileka, S.; Scott, C.; James, K.; Buddenborg, S. K.; Berger, D. J.; Patel, G.; Garcia-Casado, M. V.; Dibling, T.; McGuigan, S.; Rogers, H. A.; Hunter, A. D.; Souster, E.; Neaverson, A. S.; Goodfellow, I.; Pybus, O. G. Evaluating the Effects of SARS-CoV-2 Spike Mutation D614G on Transmissibility and Pathogenicity. *Cell* **2021**, *184* (1), 64-75.e11. https://doi.org/10.1016/j.cell.2020.11.020.

(13) Obermeyer, F.; Jankowiak, M.; Barkas, N.; Schaffner, S. F.; Pyle, J. D.; Yurkovetskiy, L.; Bosso, M.; Park, D. J.; Babadi, M.; Macinnis, B. L.; Luban, J.; Sabeti, P. C.; Lemieux, J. E. *Analysis of 6.4 Million SARS-CoV-2 Genomes Identifies Mutations Associated with Fitness*. https://www.science.org.

(14) WHO. *WHO announces simple, easy-to-say labels for SARS-CoV-2 Variants of Interest and Concern*. https://www.who.int/news/item/31-05-2021-who-announces-simple-easy-to-say-labels-for-sars-cov-2-variants-of-interest-and-concern (accessed 2023-06-01).

(15) Ellen Callaway. Heavily Mutated Omicron Variant Puts Scientists on Alert. *Nature* **2021**, *600*, 21.

(16) Chatterjee, S.; Bhattacharya, M.; Nag, S.; Dhama, K.; Chakraborty, C. A Detailed Overview of SARS-CoV-2 Omicron: Its Sub-Variants, Mutations and Pathophysiology, Clinical Characteristics, Immunological Landscape, Immune Escape, and Therapies. *Viruses*. NLM (Medline) January 5, 2023. https://doi.org/10.3390/v15010167.

(17) *Weekly epidemiological update on COVID-19 - 11 May 2023*. https://www.who.int/publications/m/item/weekly-epidemiological-update-on-covid-19---11-may-2023 (accessed 2023-05-12).

(18) Dhawan, M.; Saied, A. R. A.; Mitra, S.; Alhumaydhi, F. A.; Emran, T. Bin; Wilairatana, P. Omicron Variant (B.1.1.529) and Its Sublineages: What Do We Know so Far amid the Emergence of Recombinant Variants of SARS-CoV-2? *Biomedicine and Pharmacotherapy*. Elsevier Masson s.r.l. October 1, 2022. https://doi.org/10.1016/j.biopha.2022.113522.

(19) Cao, Y.; Jian, F.; Wang, J.; Yu, Y.; Song, W.; Yisimayi, A.; Wang, J.; An, R.; Chen, X.; Zhang, N.; Wang, Y.; Wang, P.; Zhao, L.; Sun, H.; Yu, L.; Yang, S.; Niu, X.; Xiao, T.; Gu, Q.; Shao, F.; Hao, X.; Xu, Y.; Jin, R.; Shen, Z.; Wang, Y.; Xie, X. S. Imprinted SARS-CoV-2 Humoral Immunity Induces Convergent Omicron RBD Evolution. *Nature* **2023**, *614* (7948), 521–529. https://doi.org/10.1038/s41586-022-05644-7.

(20) Khatri, R.; Siddqui, G.; Sadhu, S.; Maithil, V.; Vishwakarma, P.; Lohiya, B.; Goswami, A.; Ahmed, S.; Awasthi, A.; Samal, S. Intrinsic D614G and P681R/H Mutations in SARS-CoV-2 VoCs Alpha, Delta, Omicron and Viruses with D614G plus Key Signature Mutations in Spike Protein Alters Fusogenicity and Infectivity. *Med Microbiol Immunol* **2023**, *212* (1), 103–122. https://doi.org/10.1007/s00430-022-00760-7.

(21) Uriu, K.; Ito, J.; Zahradnik, J.; Fujita, S.; Kosugi, Y.; Schreiber, G.; Sato, K. Enhanced Transmissibility, Infectivity, and Immune Resistance of the SARS-CoV-2 Omicron XBB.1.5 Variant. *The Lancet Infectious Diseases*. Elsevier Ltd March 1, 2023, pp 280–281. https://doi.org/10.1016/S1473-3099(23)00051-8.

(22) Zappa, M.; Verdecchia, P.; Angeli, F. Is the Competition between Variants the End of Severe Acute Respiratory Syndrome Coronavirus 2 Pandemic? A Journey from Wuhan to XBB.1.16. *Eur J Intern Med* **2023**. https://doi.org/10.1016/j.ejim.2023.04.016.

(23) Zhao, Y.; Chen, F.; Li, Q.; Wang, L.; Fan, C. Isothermal Amplification of Nucleic Acids. *Chemical Reviews*. American Chemical Society November 25, 2015, pp 12491–12545. https://doi.org/10.1021/acs.chemrev.5b00428.

(24) Piepenburg, O.; Williams, C. H.; Stemple, D. L.; Armes, N. A. DNA Detection Using Recombination Proteins. *PLoS Biol* **2006**, *4* (7), 1115–1121. https://doi.org/10.1371/journal.pbio.0040204.

(25) Bianco, P. R. *Mechanistic Studies of Stalled DNA Replication Fork Rescue View Project*; 1998. https://www.researchgate.net/publication/13652960.

(26) Cabada, M. M.; Malaga, J. L.; Castellanos-Gonzalez, A.; Bagwell, K. A.; Naeger, P. A.; Rogers, H. K.; Maharsi, S.; Mbaka, M.; Clinton White, A. Recombinase Polymerase Amplification Compared to

Real-Time Polymerase Chain Reaction Test for the Detection of Fasciola Hepatica in Human Stool. *American Journal of Tropical Medicine and Hygiene* **2017**, *96* (2), 341–346. https://doi.org/10.4269/ajtmh.16-0601.

(27) Kersting, S.; Rausch, V.; Bier, F. F.; Von Nickisch-Rosenegk, M. Rapid Detection of Plasmodium Falciparum with Isothermal Recombinase Polymerase Amplification and Lateral Flow Analysis. *Malar J* **2014**, *13* (1). https://doi.org/10.1186/1475-2875-13-99.

(28) Wu, Y. D.; Zhou, D. H.; Zhang, L. X.; Zheng, W. Bin; Ma, J. G.; Wang, M.; Zhu, X. Q.; Xu, M. J. Recombinase Polymerase Amplification (RPA) Combined with Lateral Flow (LF) Strip for Equipment-Free Detection of Cryptosporidium Spp. Oocysts in Dairy Cattle Feces. *Parasitol Res* **2016**, *115* (9), 3551–3555. https://doi.org/10.1007/s00436-016-5120-4.

(29) Boyle, D. S.; McNerney, R.; Teng Low, H.; Leader, B. T.; Pérez-Osorio, A. C.; Meyer, J. C.; O'Sullivan, D. M.; Brooks, D. G.; Piepenburg, O.; Forrest, M. S. Rapid Detection of Mycobacterium Tuberculosis by Recombinase Polymerase Amplification. *PLoS One* **2014**, *9* (8). https://doi.org/10.1371/journal.pone.0103091.

(30) Yang, M.; Ke, Y.; Wang, X.; Ren, H.; Liu, W.; Lu, H.; Zhang, W.; Liu, S.; Chang, G.; Tian, S.; Wang, L.; Huang, L.; Liu, C.; Yang, R.; Chen, Z. Development and Evaluation of a Rapid and Sensitive EBOV-RPA Test for Rapid Diagnosis of Ebola Virus Disease. *Sci Rep* **2016**, *6*. https://doi.org/10.1038/srep26943.

(31) Sun, N.; Wang, W.; Wang, J.; Yao, X.; Chen, F.; Li, X.; Yinglei, Y.; Chen, B. Reverse Transcription Recombinase Polymerase Amplification with Lateral Flow Dipsticks for Detection of Influenza A Virus and Subtyping of H1 and H3. *Mol Cell Probes* **2018**, *42*, 25–31. https://doi.org/10.1016/j.mcp.2018.10.004.

(32) Patel, P.; Abd El Wahed, A.; Faye, O.; Prüger, P.; Kaiser, M.; Thaloengsok, S.; Ubol, S.; Sakuntabhai, A.; Leparc-Goffart, I.; Hufert, F. T.; Sall, A. A.; Weidmann, M.; Niedrig, M. A Field-Deployable Reverse Transcription Recombinase Polymerase Amplification Assay for Rapid Detection of the Chikungunya Virus. *PLoS Negl Trop Dis* **2016**, *10* (9). https://doi.org/10.1371/journal.pntd.0004953.

(33) García-Bernalt Diego, J.; Fernández-Soto, P.; Muro, A. The Future of Point-of-Care Nucleic Acid Amplification Diagnostics after COVID-19: Time to Walk the Walk. *International Journal of Molecular Sciences*. MDPI November 1, 2022. https://doi.org/10.3390/ijms232214110.

(34) Yang, J.; Hu, X.; Wang, W.; Yang, Y.; Zhang, X.; Fang, W.; Zhang, L.; Li, S.; Gu, B. RT-LAMP Assay for Rapid Detection of the R203M Mutation in SARS-CoV-2 Delta Variant. *Emerg Microbes Infect* **2022**, *11* (1), 978–987. https://doi.org/10.1080/22221751.2022.2054368.

(35) Tang, G.; Zhang, Z.; Tan, W.; Long, F.; Sun, J.; Li, Y.; Zou, S.; Yang, Y.; Cai, K.; Li, S.; Wang, Z.; Liu, J.; Mao, G.; Ma, Y.; Zhao, G.-P.; Tian, Z.-G.; Zhao, W. RT-RPA-Cas12a-Based Assay Facilitates the Discrimination of SARS-CoV-2 Variants of Concern. *Sens Actuators B Chem* **2023**, *381*, 133433. https://doi.org/https://doi.org/10.1016/j.snb.2023.133433.

(36) Zhao, C.; Yang, L.; Zhang, X.; Tang, Y.; Wang, Y.; Shao, X.; Gao, S.; Liu, X.; Wang, P. Rapid and Sensitive Genotyping of SARS-CoV-2 Key Mutation L452R with an RPA-PfAgo Method. *Anal Chem* **2022**, *94* (49), 17151–17159. https://doi.org/10.1021/acs.analchem.2c03563.

(37) Notomi, T.; Okayama, H.; Masubuchi, H.; Yonekawa, T.; Watanabe, K.; Amino, N.; Hase, T. *Loop-Mediated Isothermal Amplification of DNA*; 2000; Vol. 28.

(38) Chaouch, M. Loop-Mediated Isothermal Amplification (LAMP): An Effective Molecular Point-of-Care Technique for the Rapid Diagnosis of Coronavirus SARS-CoV-2. *Reviews in Medical Virology*. John Wiley and Sons Ltd November 1, 2021. https://doi.org/10.1002/rmv.2215.

(39) Li, J.; Macdonald, J.; Von Stetten, F. Review: A Comprehensive Summary of a Decade Development of the Recombinase Polymerase Amplification. *Analyst*. Royal Society of Chemistry January 7, 2019, pp 31–67. https://doi.org/10.1039/c8an01621f.

(40) Wong, Y. P.; Othman, S.; Lau, Y. L.; Radu, S.; Chee, H. Y. Loop-Mediated Isothermal Amplification (LAMP): A Versatile Technique for Detection of Micro-Organisms. *Journal of Applied Microbiology*. March 1, 2018, pp 626–643. https://doi.org/10.1111/jam.13647.

(41) Zou, Y.; Mason, M. G.; Botella, J. R. Evaluation and Improvement of Isothermal Amplification Methods for Point-of-Need Plant Disease Diagnostics. *PLoS One* **2020**, *15* (6 June). https://doi.org/10.1371/journal.pone.0235216.

(42) Zaghloul, H.; El-Shahat, M. Recombinase Polymerase Amplification as a Promising Tool in Hepatitis C Virus Diagnosis. *World Journal of Hepatology*. Baishideng Publishing Group Co 2014, pp 916–922. https://doi.org/10.4254/wjh.v6.i12.916.

(43) Kevadiya, B. D.; Machhi, J.; Herskovitz, J.; Oleynikov, M. D.; Blomberg, W. R.; Bajwa, N.; Soni, D.; Das, S.; Hasan, M.; Patel, M.; Senan, A. M.; Gorantla, S.; McMillan, J. E.; Edagwa, B.; Eisenberg, R.; Gurumurthy, C. B.; Reid, S. P. M.; Punyadeera, C.; Chang, L.; Gendelman, H. E. Diagnostics for SARS-CoV-2 Infections. *Nature Materials*. Nature Research May 1, 2021, pp 593–605. https://doi.org/10.1038/s41563-020-00906-z.

(44) Kwok, H. F. The Significance of Advanced COVID-19 Diagnostic Testing in Pandemic Control Measures. *International Journal of Biological Sciences*. Ivyspring International Publisher 2022, pp 4610–4617. https://doi.org/10.7150/ijbs.72837.

(45) Abdelmajeed, N.; Hadar, G. B.; G, W. D.; Esther, O.-D.; Sheera, A. Identification of SARS-CoV-2 Variants of Concern Using Amplicon Next-Generation Sequencing. *Microbiol Spectr* **2022**, *10* (4), e00736-22. https://doi.org/10.1128/spectrum.00736-22.

(46) Focosi, D.; Quiroga, R.; McConnell, S.; Johnson, M. C.; Casadevall, A. Convergent Evolution in SARS-CoV-2 Spike Creates a Variant Soup from Which New COVID-19 Waves Emerge. *Int J Mol Sci* **2023**, *24* (3), 2264. https://doi.org/10.3390/ijms24032264.

(47) Brito, A. F.; Semenova, E.; Dudas, G.; Hassler, G. W.; Kalinich, C. C.; Kraemer, M. U. G.; Ho, J.; Tegally, H.; Githinji, G.; Agoti, C. N.; Matkin, L. E.; Whittaker, C.; Howden, B. P.; Sintchenko, V.; Zuckerman, N. S.; Mor, O.; Blankenship, H. M.; de Oliveira, T.; Lin, R. T. P.; Siqueira, M. M.; Resende, P. C.; Vasconcelos, A. T. R.; Spilki, F. R.; Aguiar, R. S.; Alexiev, I.; Ivanov, I. N.; Philipova, I.;

Carrington, C. V. F.; Sahadeo, N. S. D.; Branda, B.; Gurry, C.; Maurer-Stroh, S.; Naidoo, D.; von Eije, K. J.; Perkins, M. D.; van Kerkhove, M.; Hill, S. C.; Sabino, E. C.; Pybus, O. G.; Dye, C.; Bhatt, S.; Flaxman, S.; Suchard, M. A.; Grubaugh, N. D.; Baele, G.; Faria, N. R. Global Disparities in SARS-CoV-2 Genomic Surveillance. *Nat Commun* **2022**, *13* (1), 7003. https://doi.org/10.1038/s41467-022-33713-y.

(48) Ong, D. S. Y.; Koeleman, J. G. M.; Vaessen, N.; Breijer, S.; Paltansing, S.; de Man, P. Rapid Screening Method for the Detection of SARS-CoV-2 Variants of Concern. *Journal of Clinical Virology* **2021**, *141*, 104903. https://doi.org/https://doi.org/10.1016/j.jcv.2021.104903.

(49) Huanyu, W.; Sophonie, J.; Richard, E.; John, M.; Pamela, S.; Huolin, T.; M, J. D.; L, L. A. Mutation-Specific SARS-CoV-2 PCR Screen: Rapid and Accurate Detection of Variants of Concern and the Identification of a Newly Emerging Variant with Spike L452R Mutation. *J Clin Microbiol* **2021**, *59* (8), e00926-21. https://doi.org/10.1128/JCM.00926-21.

(50) Chung, H.-Y.; Jian, M.; Chang, C.-K.; Chen, C.-S.; Li, S.-Y.; Lin, J.-C.; Yeh, K.-M.; Yang, Y.-S.; Chen, C.-W.; Hsieh, S.-S.; Tang, S.-H.; Perng, C.-L.; Hung, K.-S.; Chang, F.-Y.; Shang, H.-S. The Application of a Novel 5-in-1 Multiplex Reverse Transcriptase–Polymerase Chain Reaction Assay for Rapid Detection of SARS-CoV-2 and Differentiation between Variants of Concern. *International Journal of Infectious Diseases* **2023**, *127*, 56–62. https://doi.org/https://doi.org/10.1016/j.ijid.2022.11.027.

(51) Yamayoshi, S.; Sakai-Tagawa, Y.; Koga, M.; Akasaka, O.; Nakachi, I.; Koh, H.; Maeda, K.; Adachi, E.; Saito, M.; Nagai, H.; Ikeuchi, K.; Ogura, T.; Baba, R.; Fujita, K.; Fukui, T.; Ito, F.; Hattori, S. I.; Yamamoto, K.; Nakamoto, T.; Furusawa, Y.; Yasuhara, A.; Ujie, M.; Yamada, S.; Ito, M.; Mitsuya, H.; Omagari, N.; Yotsuyanagi, H.; Iwatsuki-Horimoto, K.; Imai, M.; Kawaoka, Y. Comparison of Rapid Antigen Tests for Covid-19. *Viruses* **2020**, *12* (12). https://doi.org/10.3390/v12121420.

(52) Frediani, J. K.; Levy, J. M.; Rao, A.; Bassit, L.; Figueroa, J.; Vos, M. B.; Wood, A.; Jerris, R.; Leung-Pineda, V.; Gonzalez, M. D.; Rogers, B. B.; Mavigner, M.; Schinazi, R. F.; Schoof, N.; Waggoner, J. J.; Kempker, R. R.; Rebolledo, P. A.; O'Neal, J. W.; Stone, C.; Chahroudi, A.; Morris, C. R.; Suessmith, A.; Sullivan, J.; Farmer, S.; Foster, A.; Roback, J. D.; Ramachandra, T.; Washington, C.; Le, K.; Cordero, M. C.; Esper, A.; Nehl, E. J.; Wang, Y. F.; Tyburski, E. A.; Martin, G. S.; Lam, W. A. Multidisciplinary Assessment of the Abbott BinaxNOW SARS-CoV-2 Point-of-Care Antigen Test in the Context of Emerging Viral Variants and Self-Administration. *Sci Rep* **2021**, *11* (1), 14604. https://doi.org/10.1038/s41598-021-94055-1.

(53) Shirato, K.; Nao, N.; Katano, H.; Takayama, I.; Saito, S.; Kato, F.; Katoh, H.; Sakata, M.; Nakatsu, Y.; Mori, Y.; Kageyama, T.; Matsuyama, S.; Takeda, M. Development of Genetic Diagnostic Methods for Detection for Novel Coronavirus 2019(NCoV-2019) in Japan. *Jpn J Infect Dis* **2020**, *73* (4), 304–307. https://doi.org/10.7883/yoken.JJID.2020.061.

(54) Ye, J.; Coulouris, G.; Zaretskaya, I.; Cutcutache, I.; Rozen, S.; Madden, T. L. Primer-BLAST: A Tool to Design Target-Specific Primers for Polymerase Chain Reaction. *BMC Bioinformatics* **2012**, *13* (1), 134. https://doi.org/10.1186/1471-2105-13-134.

(55) Elbe, S.; Buckland-Merrett, G. Data, Disease and Diplomacy: GISAID's Innovative Contribution to Global Health. *Global Challenges* **2017**, *1* (1), 33–46. https://doi.org/10.1002/gch2.1018.

(56) O'Toole, Á.; Scher, E.; Underwood, A.; Jackson, B.; Hill, V.; McCrone, J. T.; Colquhoun, R.; Ruis, C.; Abu-Dahab, K.; Taylor, B.; Yeats, C.; du Plessis, L.; Maloney, D.; Medd, N.; Attwood, S. W.; Aanensen, D. M.; Holmes, E. C.; Pybus, O. G.; Rambaut, A. Assignment of Epidemiological Lineages in an Emerging Pandemic Using the Pangolin Tool. *Virus Evol* **2021**, *7* (2). https://doi.org/10.1093/ve/veab064.

(57) Kumar, S.; Stecher, G.; Tamura, K. MEGA7: Molecular Evolutionary Genetics Analysis Version 7.0 for Bigger Datasets. *Mol Biol Evol* **2016**, *33* (7), 1870–1874. https://doi.org/10.1093/MOLBEV/MSW054.

(58) Prediger, E. *Calculations: Converting from nanograms to copy number*. https://sg.idtdna.com/pages/education/decoded/article/calculations-converting-from-nanograms-to-copy-number (accessed 2023-04-05).

(59) MGHD. *Universal Lateral Flow Dipstick for the Detection of Biotin-and FITC-Labeled Analytes (Proteins, Genomic Amplificates); REF*. https://www.milenia-biotec.com/uploads/2019/07/MGHD_C.pdf (accessed 2023-04-14).

(60) Magleby, R.; Westblade, L. F.; Trzebucki, A.; Simon, M. S.; Rajan, M.; Park, J.; Goyal, P.; Safford, M. M.; Satlin, M. J. Impact of Severe Acute Respiratory Syndrome Coronavirus 2 Viral Load on Risk of Intubation and Mortality among Hospitalized Patients with Coronavirus Disease 2019. *Clinical Infectious Diseases* **2021**, *73* (11), E4197–E4205. https://doi.org/10.1093/cid/ciaa851.

(61) Cherkaoui, D.; Heaney, J.; Huang, D.; Byott, M.; Miller, B. S.; Nastouli, E.; McKendry, R. A. Clinical Validation of a Rapid Variant-Proof RT-RPA Assay for the Detection of SARS-CoV-2. *Diagnostics* **2022**, *12* (5). https://doi.org/10.3390/diagnostics12051263.

(62) El Wahed, A. A.; Patel, P.; Maier, M.; Pietsch, C.; Rüster, D.; Böhlken-Fascher, S.; Kissenkötter, J.; Behrmann, O.; Frimpong, M.; Diagne, M. M.; Faye, M.; Dia, N.; Shalaby, M. A.; Amer, H.; Elgamal, M.; Zaki, A.; Ismail, G.; Kaiser, M.; Corman, V. M.; Niedrig, M.; Landt, O.; Faye, O.; Sall, A. A.; Hufert, F. T.; Truyen, U.; Liebert, U. G.; Weidmann, M. Suitcase Lab for Rapid Detection of SARS-CoV-2 Based on Recombinase Polymerase Amplification Assay. *Anal Chem* **2021**, *93* (4), 2627–2634. https://doi.org/10.1021/acs.analchem.0c04779.

(63) Liu, D.; Shen, H.; Zhang, Y.; Shen, D.; Zhu, M.; Song, Y.; Zhu, Z.; Yang, C. A Microfluidic-Integrated Lateral Flow Recombinase Polymerase Amplification (MI-IF-RPA) Assay for Rapid COVID-19 Detection. *Lab Chip* **2021**, *21* (10), 2019–2026. https://doi.org/10.1039/D0LC01222J.

(64) Loan Dao Thi, V.; Herbst, K.; Boerner, K.; Meurer, M.; Kremer, L. P.; Kirrmaier, D.; Freistaedter, A.; Papagiannidis, D.; Galmozzi, C.; Stanifer, M. L.; Boulant, S.; Klein, S.; Chlanda, P.; Khalid, D.; Barreto Miranda, I.; Schnitzler, P.; Kräusslich, H.-G.; Knop, M.; Anders, S. *A Colorimetric RT-LAMP Assay and LAMP-Sequencing for Detecting SARS-CoV-2 RNA in Clinical Samples*; 2020; Vol. 12.

(65) Sherrill-Mix, S.; Hwang, Y.; Roche, A. M.; Glascock, A.; Weiss, S. R.; Li, Y.; Haddad, L.; Deraska, P.; Monahan, C.; Kromer, A.; Graham-Wooten, J.; Taylor, L. J.; Abella, B. S.; Ganguly, A.; Collman, R. G.; Van Duyne, G. D.; Bushman, F. D. Detection of SARS-CoV-2 RNA Using RT-LAMP and Molecular Beacons. *Genome Biol* **2021**, *22* (1). https://doi.org/10.1186/s13059-021-02387-y.

(66) Muenchhoff, M.; Mairhofer, H.; Nitschko, H.; Grzimek-Koschewa, N.; Hoffmann, D.; Berger, A.; Rabenau, H.; Widera, M.; Ackermann, N.; Konrad, R.; Zange, S.; Graf, A.; Krebs, S.; Blum, H.; Sing, A.; Liebl, B.; Wölfel, R.; Ciesek, S.; Drosten, C.; Protzer, U.; Boehm, S.; Keppler, O. T. Multicentre Comparison of Quantitative PCR-Based Assays to Detect SARS-CoV-2, Germany, March 2020. *Eurosurveillance* **2020**, *25* (24). https://doi.org/10.2807/1560-7917.ES.2020.25.24.2001057.

(67) Sun, Y.; Yu, L.; Liu, C.; Ye, S.; Chen, W.; Li, D.; Huang, W. One-Tube SARS-CoV-2 Detection Platform Based on RT-RPA and CRISPR/Cas12a. *J Transl Med* **2021**, *19* (1). https://doi.org/10.1186/s12967-021-02741-5.

(68) Lau, Y. L.; Ismail, I. binti; Mustapa, N. I. binti; Lai, M. Y.; Soh, T. S. T.; Hassan, A. H.; Peariasamy, K. M.; Lee, Y. L.; Kahar, M. K. B. A.; Chong, J.; Goh, P. P. Development of a Reverse Transcription Recombinase Polymerase Amplification Assay for Rapid and Direct Visual Detection of Severe Acute Respiratory Syndrome Coronavirus 2 (SARS-CoV-2). *PLoS One* **2021**, *16* (1 January). https://doi.org/10.1371/journal.pone.0245164.

(69) Ghosh, P.; Chowdhury, R.; Hossain, M. E.; Hossain, F.; Miah, M.; Rashid, M. U.; Baker, J.; Rahman, M. Z.; Rahman, M.; Ma, X.; Duthie, M. S.; Wahed, A. A. El; Mondal, D. Evaluation of Recombinase-Based Isothermal Amplification Assays for Point-of-Need Detection of SARS-CoV-2 in Resource-Limited Settings. *International Journal of Infectious Diseases* **2022**, *114*, 105–111. https://doi.org/10.1016/j.ijid.2021.11.007.

(70) Shelite, T. R.; Uscanga-Palomeque, A. C.; Castellanos-Gonzalez, A.; Melby, P. C.; Travi, B. L. Isothermal Recombinase Polymerase Amplification-Lateral Flow Detection of SARS-CoV-2, the Etiological Agent of COVID-19. *J Virol Methods* **2021**, *296*. https://doi.org/10.1016/j.jviromet.2021.114227.

(71) Aoki, M. N.; de Oliveira Coelho, B.; Góes, L. G. B.; Minoprio, P.; Durigon, E. L.; Morello, L. G.; Marchini, F. K.; Riediger, I. N.; do Carmo Debur, M.; Nakaya, H. I.; Blanes, L. Colorimetric RT-LAMP SARS-CoV-2 Diagnostic Sensitivity Relies on Color Interpretation and Viral Load. *Sci Rep* **2021**, *11* (1). https://doi.org/10.1038/s41598-021-88506-y.

(72) Mayuramart, O.; Nimsamer, P.; Rattanaburi, S.; Chantaravisoot, N.; Khongnomnan, K.; Chansaenroj, J.; Puenpa, J.; Suntronwong, N.; Vichaiwattana, P.; Poovorawan, Y.; Payungporn, S. Detection of Severe Acute Respiratory Syndrome Coronavirus 2 and Influenza Viruses Based on CRISPR-Cas12a. *Exp Biol Med* **2021**, *246* (4), 400–405. https://doi.org/10.1177/1535370220963793.

(73) Aman, R.; Marsic, T.; Sivakrishna Rao, G.; Mahas, A.; Ali, Z.; Alsanea, M.; Al-Qahtani, A.; Alhamlan, F.; Mahfouz, M. ISCAN-V2: A One-Pot RT-RPA–CRISPR/Cas12b Assay for Point-of-Care SARS-CoV-2 Detection. *Front Bioeng Biotechnol* **2022**, *9*. https://doi.org/10.3389/fbioe.2021.800104.

(74) Schaudien, D.; Baumga¨rtner, W.; Herden, C. *High Preservation of DNA Standards Diluted in 50% Glycerol*; 2007; Vol. 16. http://journals.lww.com/moleculartpathology.

(75) Röder, B.; Frühwirth, K.; Vogl, C.; Wagner, M.; Rossmanith, P. Impact of Long-Term Storage on Stability of Standard DNA for Nucleic Acid-Based Methods. *J Clin Microbiol* **2010**, *48* (11), 4260–4262. https://doi.org/10.1128/JCM.01230-10.

(76) Kellman, B. P.; Baghdassarian, H. M.; Pramparo, T.; Shamie, I.; Gazestani, V.; Begzati, A.; Li, S.; Nalabolu, S.; Murray, S.; Lopez, L.; Pierce, K.; Courchesne, E.; Lewis, N. E. Multiple Freeze-Thaw Cycles Lead to a Loss of Consistency in Poly(A)-Enriched RNA Sequencing. *BMC Genomics* **2021**, *22* (1). https://doi.org/10.1186/s12864-021-07381-z.

(77) Brian, D. A.; Baric, R. S. *Coronavirus Genome Structure and Replication*; Springer-Verlag, 2005; Vol. 287.

(78) Bruner, K. M.; Wang, Z.; Simonetti, F. R.; Bender, A. M.; Kwon, K. J.; Sengupta, S.; Fray, E. J.; Beg, S. A.; Antar, A. A. R.; Jenike, K. M.; Bertagnolli, L. N.; Capoferri, A. A.; Kufera, J. T.; Timmons, A.; Nobles, C.; Gregg, J.; Wada, N.; Ho, Y. C.; Zhang, H.; Margolick, J. B.; Blankson, J. N.; Deeks, S. G.; Bushman, F. D.; Siliciano, J. D.; Laird, G. M.; Siliciano, R. F. A Quantitative Approach for Measuring the Reservoir of Latent HIV-1 Proviruses. *Nature* **2019**, *566* (7742), 120–125. https://doi.org/10.1038/s41586-019-0898-8.

(79) Yoshioka, K.; Kakumu, S.; Wakita, T.; Ishikawa, T.; Itoh, Y.; Takayanagi, M.; Higashi, Y.; Shibata, M.; Morishima, T. Detection of Hepatitis C Virus by Polymerase Chain Reaction and Response to Interferon-α Therapy: Relationship to Genotypes of Hepatitis C Virus. *Hepatology* **1992**, *16* (2), 293–299. https://doi.org/10.1002/hep.1840160203.

(80) Savino, S.; Desmet, T.; Franceus, J. Insertions and Deletions in Protein Evolution and Engineering. *Biotechnology Advances*. Elsevier Inc. November 1, 2022. https://doi.org/10.1016/j.biotechadv.2022.108010.

(81) Cantoni, D.; Murray, M. J.; Kalemera, M. D.; Dicken, S. J.; Stejskal, L.; Brown, G.; Lytras, S.; Coey, J. D.; McKenna, J.; Bridgett, S.; Simpson, D.; Fairley, D.; Thorne, L. G.; Reuschl, A.; Forrest, C.; Ganeshalingham, M.; Muir, L.; Palor, M.; Jarvis, L.; Willett, B.; Power, U. F.; McCoy, L. E.; Jolly, C.; Towers, G. J.; Doores, K. J.; Robertson, D. L.; Shepherd, A. J.; Reeves, M. B.; Bamford, C. G. G.; Grove, J. Evolutionary Remodelling of N-terminal Domain Loops Fine-tunes SARS-CoV -2 Spike . *EMBO Rep* **2022**, *23* (10). https://doi.org/10.15252/embr.202154322.

(82) Menéndez-Arias, L.; Matamoros, T.; Cases-González, C. E. *Insertions and Deletions in HIV-1 Reverse Transcriptase: Consequences for Drug Resistance and Viral Fitness*; 2006; Vol. 12.

(83) Migueres, M.; Lhomme, S.; Trémeaux, P.; Dimeglio, C.; Ranger, N.; Latour, J.; Dubois, M.; Nicot, F.; Miedouge, M.; Mansuy, J. M.; Izopet, J. Evaluation of Two RT-PCR Screening Assays for Identifying SARS-CoV-2 Variants. *Journal of Clinical Virology* **2021**, *143*. https://doi.org/10.1016/j.jcv.2021.104969.

(84) Ao, D.; He, X.; Hong, W.; Wei, X. The Rapid Rise of SARS-CoV-2 Omicron Subvariants with Immune Evasion Properties: XBB.1.5 and BQ.1.1 Subvariants. *MedComm (Beijing)* **2023**, *4* (2). https://doi.org/10.1002/mco2.239.

(85) Babu, B.; Ochoa-Corona, F. M.; Paret, M. L. Recombinase Polymerase Amplification Applied to Plant Virus Detection and Potential Implications. *Anal Biochem* **2018**, *546*, 72–77. https://doi.org/10.1016/j.ab.2018.01.021.

11. Acknowledgments

I would like to express my sincere gratitude to Dr. Hitoshi Oshitani for his unwavering support and guidance during my Ph.D. studies at the Department of Virology, Graduate School of Medicine, Tohoku University. I greatly admired his unique teaching approach, which encouraged students to actively engage in discussions to explore and find solutions to some of the challenges in the field of medicine. This experience has been inspiring and will serve as an example when I embark on my own teaching journey in the future. I am grateful for his emphasis on the real-world application of knowledge for the benefit of society. Furthermore, I am thankful for his confidence in me and for allowing me to work on my project even when the results were uncertain.

I want to express my deep gratitude to Dra. Mayuko Saito for her invaluable support, feedback, and patience. Her constructive criticism has helped me improve both professionally and personally. I am particularly grateful for her assistance in facilitating communication with Dr. Oshitani and the lab staff. Moreover, her mentorship in planning, organizing, and developing writing skills for the manuscript and thesis has been immensely beneficial, and I will continue to utilize these skills in the future. I appreciate her trust in me and her willingness to support my work, even during difficult moments or when the results were uncertain.

I am grateful to Dra. Michiko Okamoto for her guidance during the crucial experimental phase of my research. Her solid experience, advice, and support were invaluable. I would also like to express my gratitude to Dra. Monica Pajuelo, Dr. Pablo Tsukayama, Lucero Mascaro, Diego Bernhard Cuicapuza Arteaga, and Henry Torres of the Universidad Peruana Cayetano Heredia for their willingness and confidence in collaborating, which was crucial support in my research.

Similarly, I want to extend my gratitude to Dr. Emmanuel Kagning Tsinda, Dr. Kanako Otani, Dr. Masamichi Katsumi, Dr. Kazuhisa Kawamura, Dr. Hidekazu Nishimura, Dr. Akie Sakagami, Dr. Yo Ueki, Dr. Suguru Omiya, Dr. Satoshi Okamoto, Dr. Asami Nakayama, Dr. Shin-ichi Fujimaki, Prof. Chuyao Yu, Prof. Sikandar Azam, Dr. Eiichi Kodama, and Dr. Clyde Dapat for their contributions and support.

I would also like to express my gratitude to Dra. Mariko Saito, Makiko Kishi, Yuki Kabeya, Dr. Masahiro Sakamoto, Izumi Suzuki, Cheng Chen, Abe Sumie, and Midori Okabe for their technical, administrative, and personal support.

I want to extend my gratitude to the personnel at the Japanese Embassy in Peru, the Ministry of Education, Culture, Sports, Science, and Technology Scholarship, the National Fund for Scientific, Technological Development, and Innovation (FONDECYT), Contract 045-2020, the Japan Society for the Promotion of Science Fund, KAKENHI (grant No. JP19K24679), and the Japan Agency for Medical Research and Development (AMED) (grant no. JP20wm0125001) for their generous support.

Furthermore, I want to express my heartfelt appreciation to my family for their unwavering support, which has given me strength even during the most challenging moments. I am grateful for the unconditional love and support from my mother, Victoria, sister Patricia, and Maria Mercedes. I dedicate this work to the memory of my father, Jose Luis, whose dedication to research and teaching has profoundly influenced my professional and personal life. Lastly, I dedicate this work to my daughters, Lila and Ysabella. Even in the face of tough and difficult moments, you are the reason I strive for the best and push myself to reach new heights.